TÜBİTAK

Turkish Journal of Earth Sciences

http://journals.tubitak.gov.tr/earth/

Research Article

Turkish J Earth Sci
(2021) 30: 806-832
© TÜBİTAK
doi:10.3906/yer-2109-3

Paleoseismic history of the Manisa fault zone, Western Anatolia

İsmail DURAN[1], Hasan SÖZBİLİR[2,3], Semih ESKİ[1,2], Mustafa SOFTA[2,*], Hüseyin UYTUN[4], Mehmet YÜKSEL[5], Mustafa TOPAKSU[5]

[1]The Graduate of Natural and Applied Sciences, Applied Geology, Dokuz Eylül University, İzmir, Turkey
[2]Department of Geological Engineering, Faculty of Engineering, Dokuz Eylül University, İzmir, Turkey
[3]Earthquake Research and Implementation Center of Dokuz Eylül University, İzmir, Turkey
[4]Investment Monitoring and Coordination Directorate, İzmir Governorship, Manisa, Turkey
[5]Department of Physics, Faculty of Arts-Sciences, Çukurova University, Adana, Turkey

Received: 10.09.2021 • **Accepted/Published Online:** 17.10.2021 • **Final Version:** 30.10.2021

Abstract: The 45-km-long, E-W to NW-SE-striking Manisa Fault Zone, which constitutes the western section of the Gediz Graben, is characterized by a pure normal sense of motion with a minor strike-slip component. Even though there are numerous historical earthquakes have been listed in Western Anatolia Graben System, a few studies have been addressed on seismic sources of the earthquakes so far. According to existing literature, the western segment of the Manisa Fault Zone is well known characterized; however, the eastern segment of it has rarely been addressed. To decipher the Holocene seismotectonic behavior of the eastern segment of Manisa Fault Zone, trench-based paleoseismological analyses for the first time were performed along with it. To constrain the timing and frequency of past earthquakes, and elapse time from the last activation using the optically stimulated luminescence (OSL) and radiocarbon (^{14}C) dating, we collected twenty-six colluvial and paleosol samples from the trenches. The obtained paleoseismic data show that (i) Manisa Fault Zone is responsible for six surface rupturing earthquakes since late Pleistocene-Holocene, which is occurred at 30.6 ± 8.8 ka (E1), 15.0 ± 5.0 ka (E2), 6.6 ± 1.3 ka (E3), 2.9 ± 1.3 ka (E4), 0.8 ± 0.4 ka (E5), and 0.1 ± 0.1 ka (E6), (ii) the recurrences interval of destructive earthquakes on Manisa Fault Zone was found between 0.95 kyr to 3.8 kyr for Holocene, and (iii) the elapsed time since the most recent surface ruptured earthquake on the Manisa Fault Zone is 159 year.

Key words: Paleoseismology, active fault, Manisa Fault Zone, Gediz Graben, western Anatolia

1. Introduction

The Western Anatolia Graben System (WAGS) (Arpat and Bingöl, 1969; Bellier et al., 1997; Akyol and Karagöz, 2009; Foumelis et al., 2021) has been prone to numerous earthquake activity since the historical periods due to convergence of the African and Eurasian plates and their slab rollback and subduction phenomenon (Ergin et al., 1967; Ambraseys and Finkel, 1995; Ambraseys and Jackson, 1998; Jolivet et al., 2013,2015; Başarır Baştürk et al., 2017), (Figure 1a). These earthquakes were produced by many active faults scattered throughout the WAGS consisting of several major graben systems such as Gediz Graben, Küçük Menderes Graben, and Büyük Menderes Graben (Dewey and Şengör, 1979; Şengör et al., 1984; Royden, 1993; Bozkurt, 2003; Jolivet and Brun; 2010; Emre et al., 2018). The southwestern rim of the Gediz Graben is bounded by Manisa Fault Zone (Paton, 1992; Seyitoğlu and Scott, 1996; Hakyemez et al., 1999; Bozkurt, 2003). Along the mountain front, the Manisa Fault Zone separates the Pleistocene-Early Holocene Emlakdere and Turgutlu formations from the footwall rocks of Bornova Flysch Zone of Late Cretaceous-Paleocene age and Neogene volcano-sedimentary units (Okay et al., 1996, Özkaymak and Sözbilir, 2012, Özkaymak et al., 2013), (Figure 2).

E-W to NW-SE-striking Manisa Fault Zone (MFZ) is made up of two main fault segments at a total of 45 km long (Emre et al., 2018). Even though previous studies are mostly concentrated on the western segment of MFZ to explain Quaternary-Holocene characteristics (Özkaymak et al., 2011; Akçar et al., 2012), the studies regarding active tectonics and paleoseismology of the eastern segment of MFZ aim to unravel the Quaternary activity, and landscape evolution has so far been rarely addressed. According to Özkaymak et al's. (2011) studies, the western segment is responsible for three paleo-earthquakes, which correspond to 926 AD, 1595 AD, or 1664 AD, with the most recent event in 1845 AD. In addition, Akçar et al. (2012) stated that two of the 17 AD, 926 AD, and 1845

* Correspondence: mustafa.softa@deu.edu.tr

This work is licensed under a Creative Commons Attribution 4.0 International License.

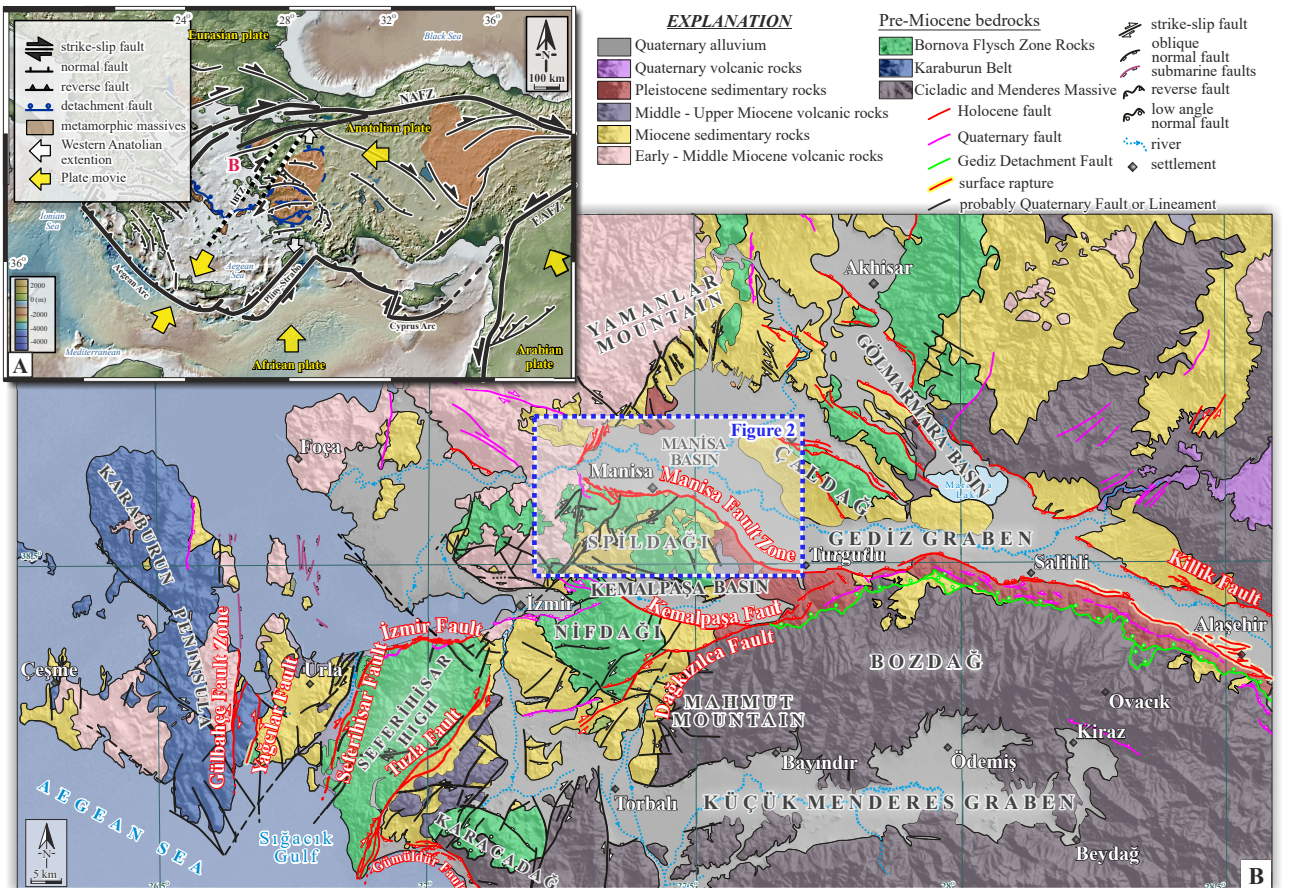


Figure 1. A) Map showing the location of the study area and the main tectonic lines in Turkey (Eski et al., 2020 adapted from Şengör et al., 1985; Barka, 1992; Bozkurt, 2001; Koçyiğit and Özacar, 2003. B) Regional-scale generalized geological map of the study area (Revised Eski et al., 2020 and adapted from; Bozkurt, 2001; Candan et al., 2011; Uzel et al., 2013; Özkaymak et al., 2013; Emre et al., 2018 and Tepe et al., 2021).

AD earthquakes seem to have produced ruptures on the Mugırtepe Fault scarp at the western segment of MFZ.

To bridge the gap in the existing literature, we aimed at the Holocene seismotectonic behavior of Manisa Fault Zone by trench-based paleoseismological surveys to reveal (i) Pleistocene and Holocene earthquake activities, (ii) average recurrence interval, and (iii) elapsed period from the last earthquake by using optically stimulated luminescence (OSL) and radiocarbon (^{14}C) dating methods.

2. Seismotectonic setting

Western Anatolia is one of the most seismically active regions in the world (Şengör et al., 1985; Taymaz et al., 1991; Seyitoğlu and Scott, 1991; Pavlides, 1996; Papazachos and Papazachou, 1997; Altunel, 1999; Koçyiğit et al., 1999; Bozkurt, 2001; Akyüz and Altunel, 2001; Caputo et al., 2004; Pavlides and Caputo, 2004; Caputo and Helly, 2008; Akyol et al., 2006). The geological and seismological studies carried out and continuing to date show that NE-SW trending strike-slip faults and NW-SE, NE-SW and E-W trending dip/oblique-slip normal faults are dominant in and around the study area. According to the research, these faults were observed to work together and were found to be the source of both earthquakes of the instrumental period and earthquakes of the historical period (Taymaz et al., 1991; Akyol et al., 2006; Zhu et al., 2006; Aktar et al., 2007; Tan et al., 2008; Sözbilir et al., 2008, 2009; Özkaymak et al., 2011; Uzel et al., 2012).

The earthquake magnitudes that these faults can generate vary from 6.3 to 6.9, starting from the Bergama Fault in the north to the Kemalpaşa Fault in the south, and vary from 5 km to 40 km in length (Emre et al., 2018). The existence of earthquakes with a magnitude of 6.0 that have occurred in and around Manisa in the last 10 years is an important indicator of the ongoing seismic activity in the region, while a number of destructive earthquakes occured in historical periods (Soysal et al., 1981; Ambraseys, 2009; Başarır Baştürk et al., 2017), (Table 1).

There are more than five earthquakes listed in catalogs which are 17 AD, 926 AD, 1595 or 1664 AD, 1845 AD, and 1862 AD earthquakes seriously affected the Manisa city (e.g., Ergin et al., 1967; Ambraseys and Finkel, 1995; Ambraseys and Jackson, 1998; Başarır Baştürk et al., 2017). Although the historical earthquake catalogs well reflect the damage dimension on the Manisa region, the seismic source of these earthquakes is still unclear. Of these earthquakes, some of these events were attributed to MFZ, the some of them have not correlated with the fault zone. There is a questionable problem that is how relied on the historical catalogs which were prepared eyewitness and uncertain location. However, in this study, according to paleoseismological trenches, robust dating results, and statistical evaluation of events were used to generate the event time interval.

One of the well-recorded earthquakes in Western Anatolia is the earthquake AD 17. It was recorded that more than 10 settlements around the Manisa settlement were damaged by this earthquake (Ambraseys, 1988; Soysal et al., 1981; Guidoboni et al., 1994; Özkaymak, 2012). Another important earthquake is the AD 926. However, the records of this earthquake are quite limited. According to the paleoseismological studies conducted in the western part of the study area, it was found that the western part of the fault was the source of the AD 1845 earthquake (Özkaymak and Sözbilir, 2012). Another earthquake in the study area is the AD November 3, 1862, earthquake. Records of this earthquake are also very limited. However, based on earthquake catalogs, it was found that this earthquake, whose intensity was given as IX, coincided with a location between Turgutlu and Manisa. After the evaluation of the last 100 instrumental periods, a list of 50 earthquakes with magnitude greater than 3 from AFAD-ERD[1] and KOERI[2] was obtained (Figure 3).

2.1. Manisa Fault Zone

The MFZ, which is one of the large-scale normal faults, developed under the influence of the extensional tectonic regime in Western Anatolia (Özkaymak and Sözbilir, 2008, 2012; Özkaymak et al., 2011; 2013). The mapping of the fault linearity was first made by Weismantel (1891). In the earthquake geography publication of Sieberg (1932), the fault segments extending from Manisa to Alaşehir are shown on the map. The Manisa Fault is shown on the map of the earthquake catalog of Pınar and Lahn (1952). In his study of the geology of the northwest of the Manisa Mountain, Oğuz (1966) mapped a fault of approximately 3 km long covering the west and east of the city center of Manisa. Ketin (1968), in his publication examining the general tectonic situation of Turkey, showed the Manisa Fault as a fault with the potential to produce earthquakes around Manisa city. Allen (1974) first defined the fault planes of the Manisa Fault. The name Manisa Fault was first given by Hancock and Barka (1987).

The Manisa Fault was divided into two segments according to Emre et al. (2018): the western and eastern part of the fault was 35 and 26 km, respectively. These segments continue directly through the city center of Manisa (Figure 3). A few studies handled with paleostress evolution of the Manisa Fault Zone and its related structures in the literature (Bozkurt and Sözbilir, 2006; Özkaymak, 2012). Bozkurt and Sözbilir (2006) suggest that the fault is a reactivated structure that once functioned as a sinistral strike-slip fault, then as a normal fault. The first movement was formed by the formation of a short E-W compression period before the onset of the modern graben Plio-Quaternary (Bozkurt and Sözbilir, 2006). The second movement has a large normal slip component combined with small strike-slip components, with the rake of the slip lines averaging 83° and showing a NE-SW directed extension (Bozkurt and Sözbilir, 2006), (Figure 4).

In the study of Özkaymak et al (2011), the MFZ was divided into three segments. The western section consists of fault segments with a length of 10 km between the villages of Kayapınar and Akgedik and roughly trending NW-SE. The central part has a length of about 10 km with a W-E extension. The eastern segment runs NW-SE direction and has a length of 15 km. Özkaymak and Sözbilir (2012) calculated the annual slip rate for three segments in their tectonic-geomorphological study on the MFZ. Accordingly, they mention that a displacement of 0.1 mm/year, 0.3 mm/year, and 0.26 mm/year occurred on the western, central, and eastern segments, respectively.

3. Methodology

3.1. Paleoseismological studies

To define the paleoseismic activity of the MFZ, five trenches were excavated on the eastern and western segment of the master fault, where there is a well-defined morphological expression of the fault scarps. While four trenches were excavated in the NE-SW direction, one of these was excavated in the NW-SE direction with a total length of 145 m and a maximum depth and width of 4 m. After the cleaning trench walls, it was gridded with horizontal and vertical strings spaced 1 m. According to McCalpin (2009), we described the exposed units labeled by numbers based on their microstratigraphic positions. Then, sedimentary boundaries and structural features were mapped in detail

[1] AFAD-ERD (Ministry of Interior Disaster and Emergency Management Presidency) (2021). Recent Earthquakes in Turkey [online]. Website https://deprem.afad.gov.tr/ddakatalogu [accessed 16 June 2021].

[2] KOERI (Boğaziçi University Kandilli Observatory and Earthquake Research Institute Regional Earthquake-Tsunami Monitoring Center) (2021). Recent Earthquakes in Turkey [online]. Website http://www.koeri.boun.edu.tr [accessed 16 June 2021].

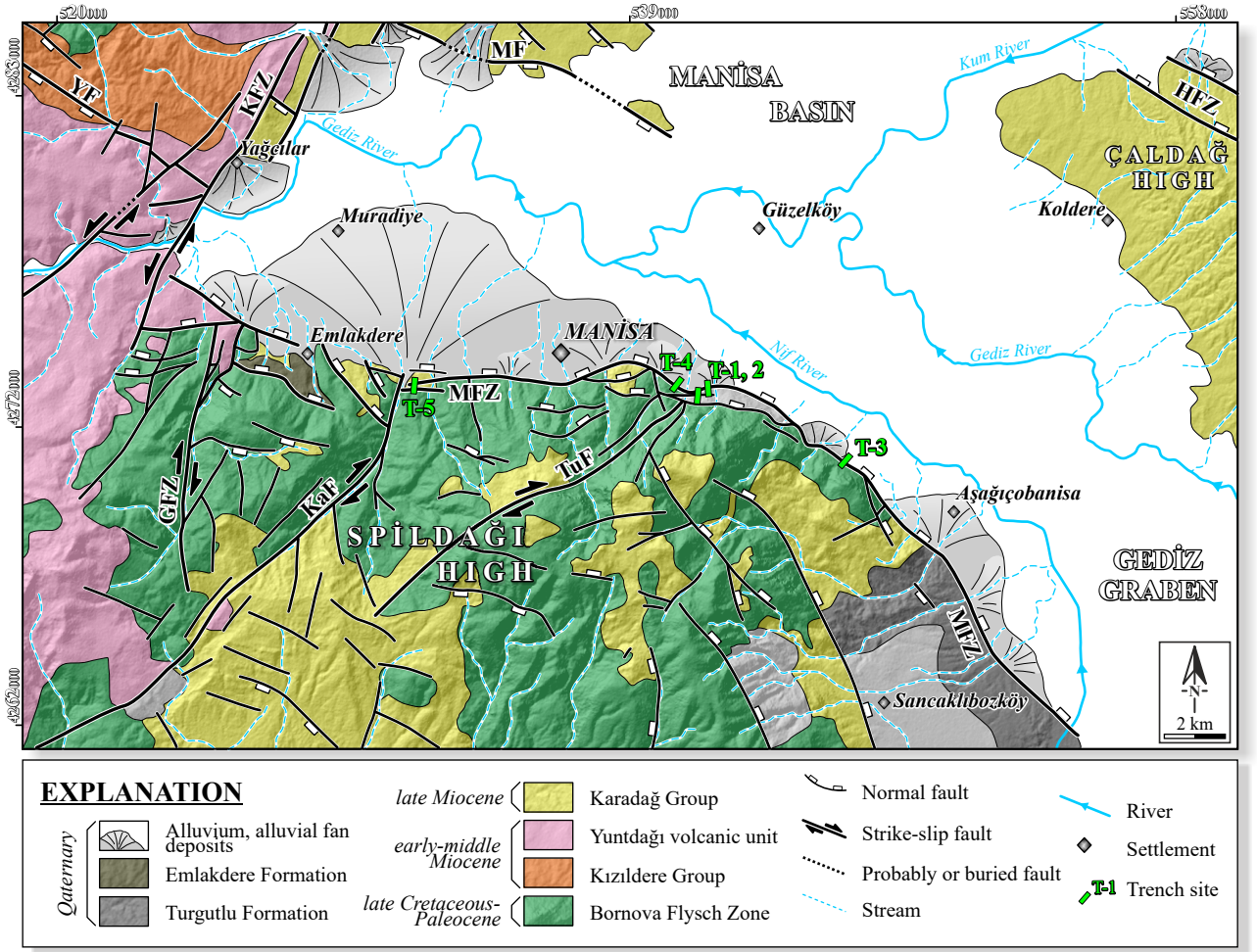


Figure 2. Geological map of the study area and trench locations (Revised from Özkaymak et al., 2013; Özkaymak and Sözbilir, 2012). Abbreviations: MFZ, Manisa Fault Zone; HFZ, Halitpaşa Fault Zone; KaF, Karaçay Fault; TuF, Turgutalp Fault; GFZ, Gürle Fault Zone; MF, Maltepe Fault; KFZ, Kaleköy Fault Zone.

with graph papers and photographs. Lastly, samples were collected for optically stimulated luminescence (OSL) and radiocarbon (^{14}C) dating of event horizons.

3.2. Dating methods

OSL and ^{14}C dating methods are one of the states of arts and well-known techniques in paleoseismological studies (e.g., Fattahi and Walker, 2007; Preusser et al., 2008; Fattahi et al., 2010; Dogan et al., 2015; Ramsey et al., 2015; Stahl et al., 2016; Tsodoulos et al., 2016). To find the timing of identified past earthquakes events related to MFZ, both OSL and ^{14}C dating methods were used. While OSL dating has enabled to direct dating of wedge and colluvium materials, ^{14}C is mostly used paleo-soils with having enough organic materials. Samples were taken from the colluvial and wedges on the walls of the trenches. Twenty-five OSL samples and one radiocarbon sample have collected the units and colluvial, wedges, and paleo-soil levels.

The samples were prepared at the Dokuz Eylül University (DEU) Sample Preparation Laboratory, and the mineral separation steps were completed according to the standard procedures described by Aitken (1998) and Spencer and Robinson (2008). The following procedures were performed for equivalent dose (D_e) and annual dose measurement procedures. The measurements of the OSL signals and its background and D_e estimations were performed at Çukurova University TL/OSL Dating Laboratory.

The D_e's of all quartz aliquots were determined using a single aliquot regenerative (SAR) dose protocol (Murray and Wintle, 2000, 2003; Wintle and Murray, 2006) (see Table 2). OSL signals were recorded using a lexsyg smart TL-OSL reader (developed by Freiberg Instruments, Richter et al., 2015), equipped with a ^{90}Sr/^{90}Y beta source (dose rate: 0.10 Gy/s) and a Hamamatsu bi-alkaline cathode photomultiplier tube (PMT). The stimulation

Table 1. List of historical earthquakes in the Manisa and surrounding area.

No	Date	Intensity	Coordinate Lat– Long	Location	References
1	AD 17	IX	38.40 – 27.50 38.5 – 27.8 38.6168 – 27.3992	Manisa (Magnesia), Muradiye, Sart (Sardes), Temnos, Myrina, Ephesus Appolania, Hyrcanis, VS Mastheni, Aegae, Hierocaesaria, Euthena, Ulloron, Philadelphia, Tmolus, Cyme, Thyatira, Gediz River, İzmir	1, 2, 3, 4, 7, 8, 9, 10, 11
2	AD 44	VIII	38.50 – 27.40	Magnesia, Ephesus	1, 2, 8, 9, 10, 11
3	AD August 8 926	VII	38.50 – 27.50	Manisa	7, 8, 9, 10, 11
4	AD September 1592	VIII	38.50 – 27.90	Turgutlu, Salihli, Manisa	2, 10, 11
5	AD September 22 1595	VII	38.50 – 27.90	Manisa, Urganlı, Sart, Ahmetli, Gedik, Bostancı, Hamza Çavuş, Azizli villages	5, 7, 8, 9, 10, 11
6	AD June 2 1664	VII	38.41 – 27.20	İzmir, Manisa	1, 2, 5, 9, 10, 11
7	AD July 10 1688	X	38.40 – 27.20	İzmir, Manisa (Magnesia), Turgutlu (Durgutli), Alaşehir (Philadephia)	2, 9, 11
8	AD September 1 1771	V	38.50 – 27.70	Aegean, Turgutlu	9, 11
9	AD September 27 1844	?	38.61 – 27.42	Manisa region, İzmir	9, 11
10	AD June 23 1845	VIII IX	38.60 – 27.50	Manisa region, İzmir	1, 2, 6, 8, 9, 10, 11, 12
11	AD April 3 1850	VIII	38.40 – 27.45	İzmir, Kemalpaşa, Turgutlu	2, 11
12	AD April 20 1850	V	38.42 – 27.42	Kemalpaşa, Manisa, İzmir, Aydın, Ödemiş, Tire, Bayındır	2, 9, 11
13	AD October 13 1850	VIII	38.40 – 27.20	İzmir, Manisa, Turgutlu, Ödemiş	2, 11
14	AD June 16 1858	VI	38.90 – 27.80	Manisa, Akhisar, İzmir	2, 9, 11
15	AD July 27 1859	?	38.61 – 27.42	Manisa	9, 11
16	AD March 4 1860	V	38.61 – 27.42	Manisa	9, 11
17	AD November 3 1862	IX	38.40 – 27.70	Turgutlu - Manisa	2, 9, 11
18	AD August 18 1866	?	38.61 – 27.42	Manisa	9, 11
19	AD November 10 1873	VI	38.92 – 27.83	Akhisar - Manisa	9, 11

References: (1) Ergin et al. (1967); (2) Soysal et al. (1981); (3) Ambraseys (1988); (4) Guidoboni et al. (1994); (5) Ambraseys and Finkel (1995); (6) Papazachos and Papazachou (1997); (7) Ambraseys and Jackson (1998); (8) Tan et al. (2008); (9) Ambraseys (2009); (10) Özkaymak et al. (2011); (11) Başarır Baştürk et al. (2017); (12) Papazachos and Papazachou (2003). AD: Anno domini.

wavelength is 458 ± 5 nm (max. 100 mW/cm^2 at sample position) for the blue light stimulation. Detection of the OSL signals was achieved using the filter pack of BSL, TL-365 nm (Hoya-U340-Glass-2,5 mm; Delta-BP 365/50 EX-Interference-5 mm).

OSL decay curves and SAR dose recovery graphs (corresponding sensitivity-corrected dose-response graph) for the selected ÇPA-3 sample are presented in Figures 5a–5b. As seen in Figure 5 (b), the ratio of the test to regenerative OSL, L_x/T_x, a sensitivity-corrected measure of the OSL response shows the linear increment of L_x/T_x with increased dose levels. The value of the R_6/R_1 rate equals 0.97 ± 0.04 for the ÇPA-3 sample, and it shows this linearity.

Environmental radioactivity dose values were determined at the laboratory of Mineral Research and Exploration General Directorate (MTA), and the annual dose values were calculated using U, Th, K ratios the samples absorbed in a year. The luminescence dates were calculated by dividing the D_e by the annual dose, according to Aitken's (1998) equation.

A ^{14}C sample taken from each trench for radiocarbon dating was meticulously collected from the paleo-soil level, which contains charred wood fragments on the trench wall. The collected sample was sent to the conventional carbon dating laboratory in Kyiv. The obtained radiocarbon result was calibrated according to Reimer et al. (2013) with the help of the OxCal program of Ramsey and Lee (2013).

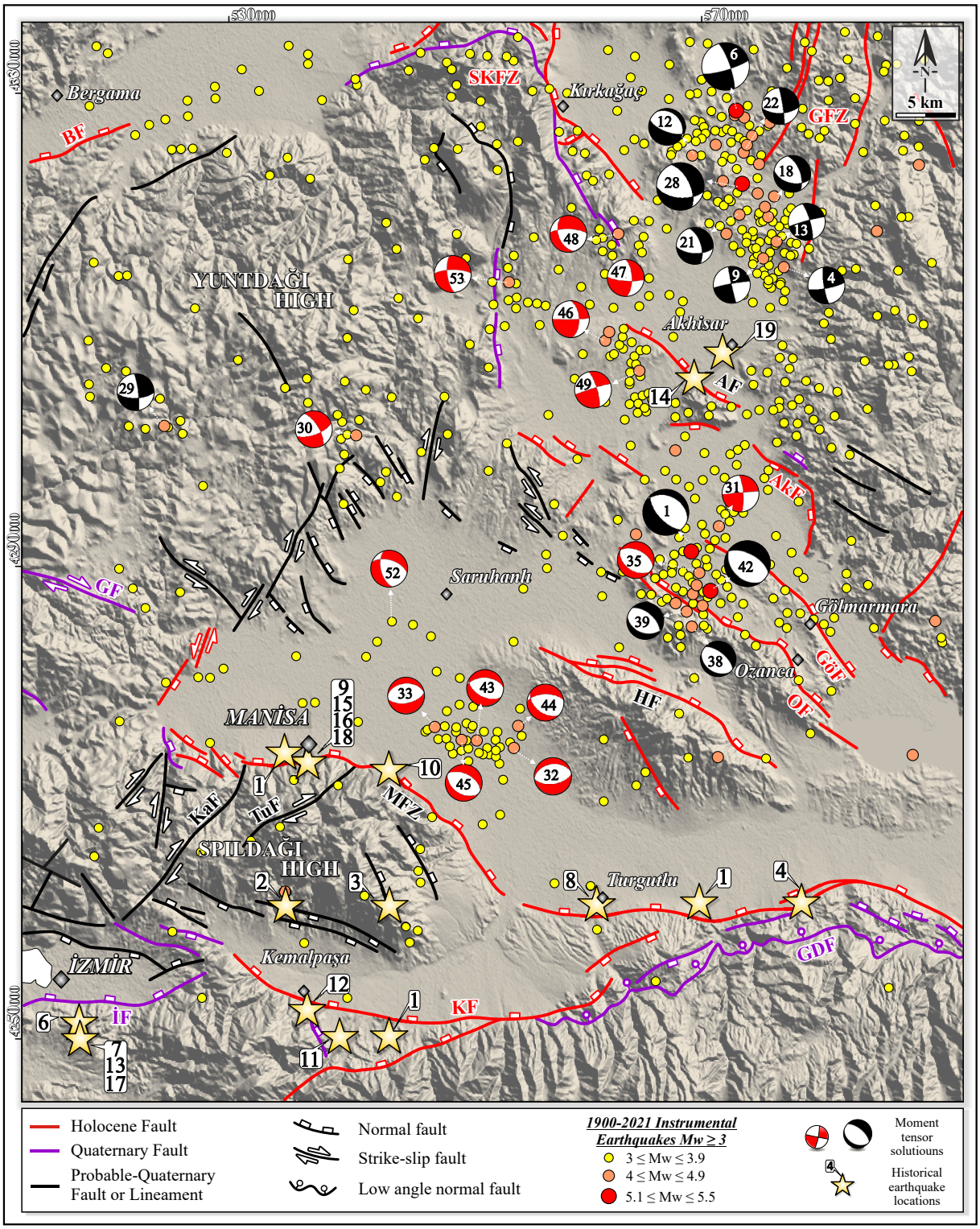


Figure 3. Seismotectonic map of Manisa region. Yellow stars indicate historical earthquakes, and yellow, orange and red dots indicate epicentres of earthquakes greater than instrumental period M≥3. Earthquake data were taken from AFAD (ERD)[1]. (The faults are taken from the following studies; Özkaymak et al., 2011; Emre et al., 2018 and Eski et al., 2020). Abbreviations: (MFZ) Manisa Fault Zone; (İF) İzmir Fault; (KF) Kemalpaşa Fault; (GDF) Gediz Detachment Fault; (KaF) Karaçay Fault; (GF) Güzelhisar Fault; (HF) Halitpaşa Fault; (OZ) Ozanca Fault; (GöF) Gölmarmara Fault; (AkF) Akselendi Fault; (AF) Akhisar Fault; (GFZ) Gelenbe Fault Zone; (SKFZ) Soma-Kırkağaç Fault Zone; (BF) Bergama Fault.

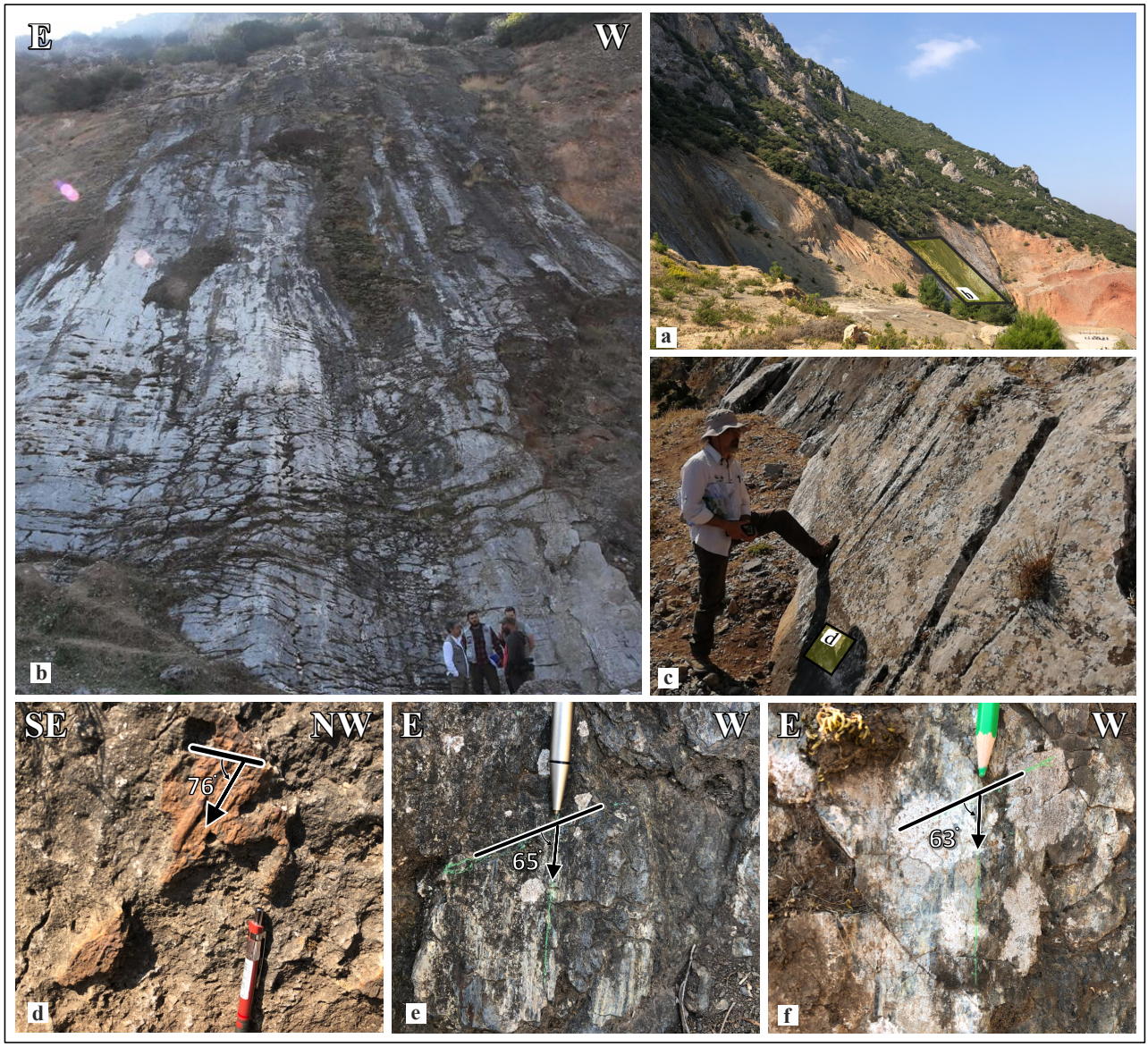


Figure 4. a-c indicates a close up view of the well-preserved Manisa Fault Zone. d-f; sub field views are showing the kinematic features that observed on the MFZ.

Moreover, gathering the robust data, OSL and ^{14}C dates were together refined by Bayesian methods in OxCal concerning historical earthquakes.

4. Findings

4.1. Paleoseismological studies

4.1.1. Trench 1

Trench 1 was excavated on the eastern segment of MFZ. It was 33 m long and up to 3.5 m deep and wide. Both trench walls have exposed eleven units with recent soil cover. The basement units consist of milky brown, unsorted, matrix-supported gravel (unit A), and greenish-brown unsorted, matrix-supported gravel (unit B). It also includes randomly distributed limestone nodules. Overlaying unit C represents light brown, matrix, and clast-supported, medium sorted, angular slope breccia. It is noted that this unit is approximately 2 m. thrown (dip-slip) due to NE and SW trending faults.

Previous units are overlaid by light brown, matrix-supported, unsorted, gravel (Unit D), dark brown organic-rich clayey mud (Unit E), whitish-beige clast supported, unsorted, angular gravel (Unit F), reddish-brown, unsorted, muddy sandy angular gravel (Unit H), dark brown muddy gravel (Unit H), light brown medium sorted muddy gravel (Unit I), milky brown unsorted, angular gravel (Unit K). The observable vertical displacement

Table 2. Applied single aliquot regeneration (SAR) protocol for quartz.

Step	Treatment	Observed
1	Preheat 220°C, 10 s	
2	Stimulation with blue LED (125°C, 80 s)	L_n
3	Give test dose	
4	Cut-heat TL (160°C, 5°C/s)	
5	Stimulation with blue LED (125°C, 80 s)	T_n
6	Give dose	Reg Point 1
7	Preheat 220°C, 10 s	
8	Stimulation with blue LED (125°C, 80 s)	L_x
9	Give test dose	
10	Cut-heat TL (160°C, 5°C/s)	
11	Stimulation with blue LED (125°C, 80 s)	T_x
12	Return to Step 6	

of Unit I is more than 2.5 m in between 29 m and 30 m of trench walls. Finally, unit L is characterized by beige gravelly recent soil cover (Figure 6).

To constrain the timing of earthquakes, a total of five OSL samples were collected from Trench 1. The calculated dates are consistent with both stratigraphic orders in the trench walls. The derived dates of the samples from trench 1 were dated between 0.67 ± 0.49 ka and 24.98 ± 5.05 ka (Table 3).

Based on the sedimentological, stratigraphic evidence the analysis of structural elements together with the results of dated samples, two events were identified in this trench. The earliest event occurred after deposition of unit G and before deposition of unit I. Hence, we collected OSL sample from the unit I (sample number ÇPÜ-4) representing the upper boundary of the first event, which yielded a date of 6.56 ± 0.55 ka, and from the unit G (sample number ÇPÜ-3) representing the lower boundary of the first event, which yielded a date of 10.65 ± 1.41 ka. The final event cuts the unit I, so it occurred after deposition of unit I and before deposition of unit K. Thus, the samples collected from the unit I yielded an OSL date of 6.56 ± 0.55 ka representing the lower boundary of the second event while the samples collected from the overlying unit (unit K, ÇPÜ-1) yielded a date between 0.67 ± 0.49 ka. In addition, the small-scaled displacements observing in unit F and unit H could be considered to include post-seismic and/or creeping motions in addition to the coseismic slip (Figure 6).

4.1.2. Trench 2

Trench 2 was located near Trench 1. It was excavated 34 m long, 3.5 m wide, and deep on the eastern segment of MFZ. Both trench walls have exposed ten units with recent soil cover. The basement unit (unit A) comprises light brown, medium sorted cement supported angular gravels. Overlying unit B consist of whitish-beige unsorted cement supported angular slope breccia. Unit A and Unit B are overlain by dark brown organic-rich clayey mud (Unit B1), milky brown- beige unsorted, coarse gravel with fine gravels lenses (Unit C), reddish-brown unsorted cement supported gravel (Unit D), light to dark brown organic-rich clayey mud (Unit H), dark brown, unsorted, muddy gravel with abrasion at some places (Unit E), dark brown, angular limestone blocky gravelly mud (Unit F), dark brown, fine to coarse gravelly mud (Unit G). In addition, unit C, unit D and unit G are evaluated as a colluvial wedge

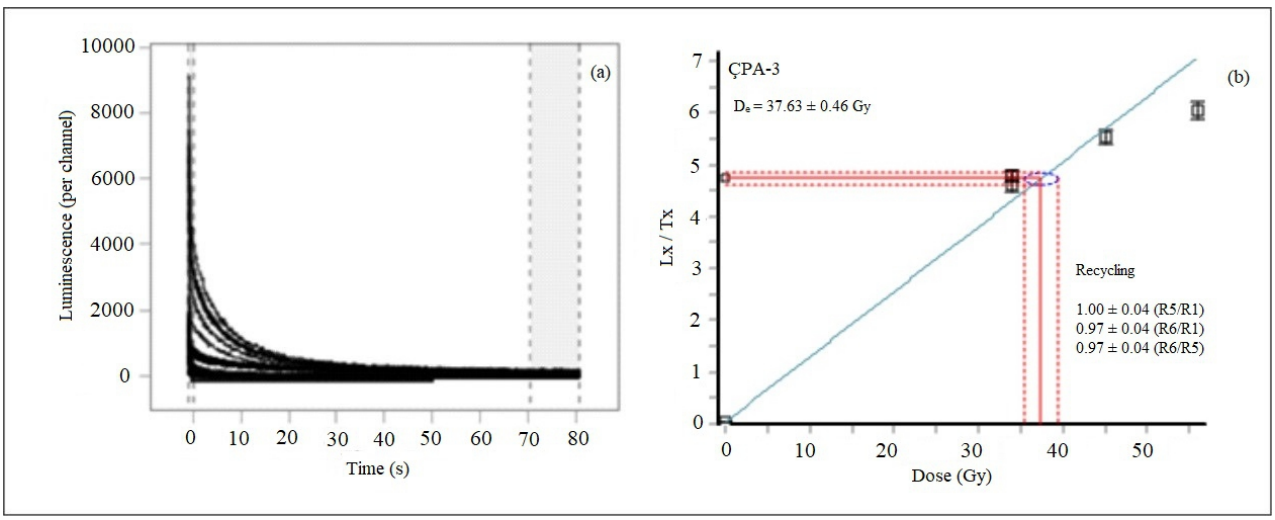
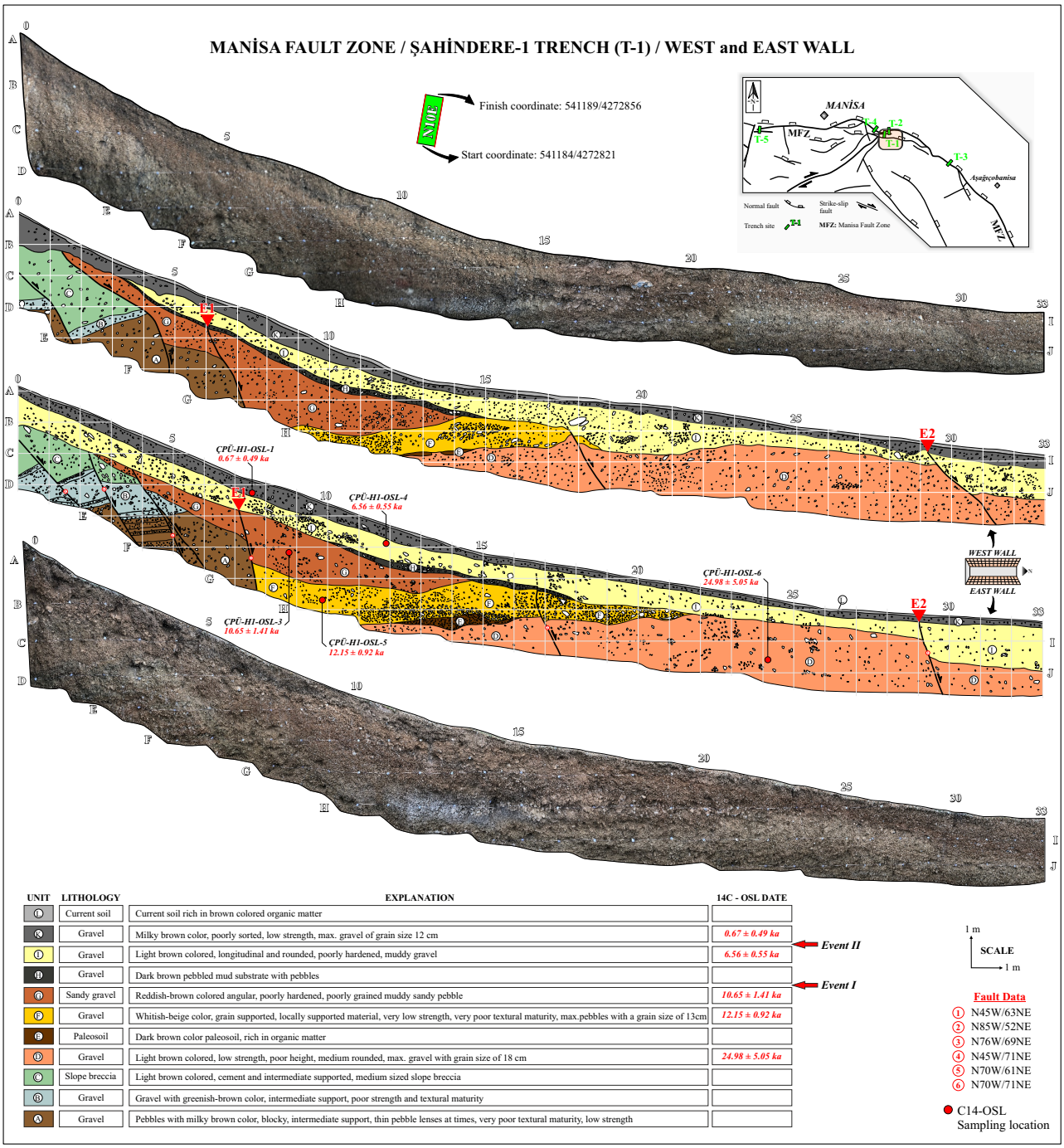


Figure 5. (a) Recorded OSL decay curves with blue light stimulation and (b) SAR dose recovery graphs of selected aliquot of quartz sample ÇPA-3.



UNIT	LITHOLOGY	EXPLANATION	14C - OSL DATE
Ⓛ	Current soil	Current soil rich in brown colored organic matter	
Ⓚ	Gravel	Milky brown color, poorly sorted, low strength, max. gravel of grain size 12 cm	0.67 ± 0.49 ka
Ⓘ	Gravel	Light brown colored, longitudinal and rounded, poorly hardened, muddy gravel	6.56 ± 0.55 ka
Ⓗ	Gravel	Dark brown pebbled mud substrate with pebbles	
Ⓖ	Sandy gravel	Reddish-brown colored angular, poorly hardened, poorly grained muddy sandy pebble	10.65 ± 1.41 ka
Ⓕ	Gravel	Whitish-beige color, grain supported, locally supported material, very low strength, very poor textural maturity, max.pebbles with a grain size of 13cm	12.15 ± 0.92 ka
Ⓔ	Paleosoil	Dark brown color paleosoil, rich in organic matter	
Ⓓ	Gravel	Light brown colored, low strength, poor height, medium rounded, max. gravel with grain size of 18 cm	24.98 ± 5.05 ka
Ⓒ	Slope breccia	Light brown colored, cement and intermediate supported, medium sized slope breccia	
Ⓑ	Gravel	Gravel with greenish-brown color, intermediate support, poor strength and textural maturity	
Ⓐ	Gravel	Pebbles with milky brown color, blocky, intermediate support, thin pebble lenses at times, very poor textural maturity, low strength	

Figure 6. Photomosaic and paleoseismological log of the trench 1. See explanation in text. Red dotted circles indicate OSL dating sample locations (The east wall is flipped).

after the relevant earthquake events. It is noted that the observable vertical displacement is more than 3 m in between 23 m and 26 m of trench walls. All these units are overlaid unconformably with light brown surface soil (Unit I) (Figure 7).

We collected a total of six OSL samples from the walls of trench 2 to constrain the timing of earthquakes. The calculated ages are consistent with both stratigraphic orders in the trench walls. The derived ages of the samples from trench 2 was dated between 3.29 ± 0.14 ka and 54.46 ± 3.07 ka (Table 3).

Based on the sedimentological, micro-stratigraphy evidence and results of dated samples, and the analysis of structural elements, three events were detected in trench

Table 3. Sample information, equivalent doses (D_e), dose rates data, and quartz OSL ages calculated for samples collected from the three trenches at MFZ.

Study Area		Sample No	Grain Size (μm)	Dose-Rate			Water Content (%)	Altitude (m)	Depth (cm)	Coordinate (Decimal Degrees)	Equivalent-Dose	Age (ka)
				^{238}U (ppm)	^{232}Th (ppm)	^{40}K (%)					D_e (Gr)	
Manisa	TRENCH 1	ÇPÜ-1	150–250	3.0	8.0	1.04	12.20	124	35	38.6037°–27.4734°	1.6 ± 1.0	0.67 ± 0.49
		ÇPÜ-3	150–250	3.7	8.1	1.12	5.12	124	220	38.6037°–27.4734°	27.8 ± 3.5	10.65 ± 1.41
		ÇPÜ-4	150–250	1.3	9.6	1.20	5.94	124	95	38.6037°–27.4734°	15.1 ± 1.1	6.56 ± 0.55
		ÇPÜ-5	150–250	5.4	3.1	0.70	5.43	124	300	38.6037°–27.4734°	27.8 ± 1.7	12.15 ± 0.92
		ÇPÜ-6	150–250	2.6	3.2	1.75	3.81	124	200	38.6037°–27.4734°	43.3 ± 8.5	24.98 ± 5.05
	TRENCH 2	ÇPA-1	150–250	2.9	10.5	1.12	7.95	85	70	38.6052°–27.4763°	63.5 ± 4.1	24.94 ± 1.90
		ÇPA-2	150–250	2.6	1.7	0.17	4.20	85	105	38.6052°–27.4763°	58.13 ± 0.51	54.46 ± 3.07
		ÇPA-3	150–250	4.9	19.5	1.78	12.13	85	70	38.6052°-27.4763°	37.63 ± 0.46	9.39 ± 0.37
		ÇPA–4	150–250	2.2	2.4	0.42	2.75	85	100	38.6052°–27.4763°	57.11 ± 0.82	44.63 ± 2.44
		ÇPA-5	150–250	3.0	22.6	2.08	16.24	85	100	38.6052°–27.4763°	38.5 ± 1.8	9.91 ± 0.58
		ÇPA-6	150–250	2.7	14.7	1.49	13.68	85	43	38.6052°–27.4763°	9.7 ± 0.2	3.29 ± 0.14
	TRENCH 3	YH-2	150–250	1.7	9.6	1.13	6.07	62	80	38.5852°–27.5276°	14.1 ± 2.3	6.21 ± 1.05
		YH-4	150–250	1.4	6.2	0.91	4.40	62	125	38.5852°–27.5276°	3.9 ± 0.3	2.17 ± 0.2
		YH-6	150–250	2.0	5.7	0.83	4.96	62	125	38.5852°–27.5276°	12.67 ± 0.58	6.18 ± 0.3
		YH-7	150–250	1.9	9.5	1.52	8.98	62	150	38.5852°–27.5276°	11.4 ± 1.1	4.42 ± 0.46
		YH-X1	150–250	1.9	9.5	1.52	8.80	62	110	38.5852°–27.5276°	8.0 ± 0.7	3.09 ± 0.3
		YH-X3	150–250	0.1	4.0	0.49	7.50	62	60	38.5852°–27.5276°	6.2 ± 0.04	6.67 ± 0.35
	TRENCH 4	MF-H2	150–250	0.6	20.8	2.70	9.57	81	155	38.6056°–27.4662°	28.6 ± 2.0	7.05 ± 0.28
		MF-H3	150–250	0.7	18.4	2.62	5.99	81	250	38.6056°–27.4662°	43.8 ± 2.8	11.01 ± 0.83
		MF-H4	150–250	1.6	19.4	2.49	11.4	81	220	38.6056°–27.4662°	27.6 ± 1.4	7.06 ± 0.45
		MF-H5	150–250	0.1	18.4	2.28	5.57	81	54	38.6056°–27.4662°	4.5 ± 0.41	1.25 ± 0.13
	TRENCH 5	GR-1	150–250	3.6	23.70	2.54	7.14	147	70	38.6057°–27.3646°	47.1 ± 1.9	9.61 ± 0.54
		GR-2	150–250	3.2	21.90	2.67	5.50	147	61	38.6057°–27.3646°	27.1 ± 4.7	5.53 ± 0.99
		GR-3	150–250	1.9	16.30	1.94	4.97	147	25	38.6057°–27.3646°	2.4 ± 0.6	0.67 ± 0.17
		GR-4	150–250	6.4	9.50	2.05	7.98	147	40	38.6057°–27.3646°	14.0 ± 3.0	3.40 ± 0.74

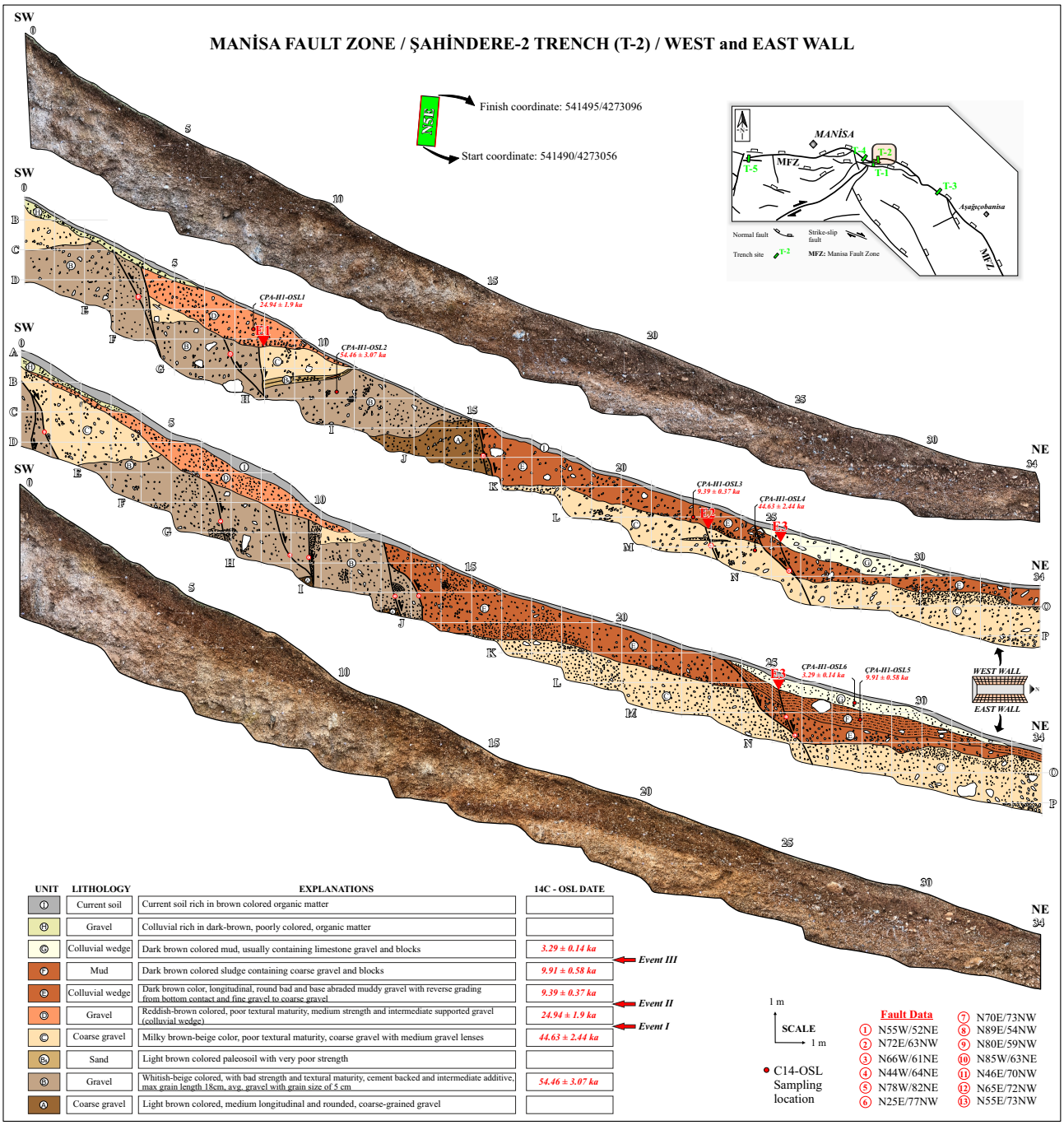


Figure 7. Photomosaic and paleoseismological log of the trench 2. See explanation in text. Red dotted circles indicate OSL dating sample locations (The east wall is flipped).

2. The first event occurred after the deposition of unit C and before the deposition of unit D. So, to define the lower boundary of the first event, we collected the ÇPA-4 sample from unit C yielded a date of 44.63 ± 2.44 ka. The age result of unit D (ÇPA-1; 24.94 ± 1.90 ka) gives the upper boundary of the first event in trench 2. The second event occurred after deposition of unit D and before deposition of unit E and Unit F. Thus, the samples collected from the unit D yielded an OSL date of 24.94 ± 1.90 ka (ÇPA-1) representing the lower boundary of the second event, while the samples collected from the overlying unit (unit E, ÇPÜ-3; unit F, ÇPA-5) yielded a date between 9.39 ±

0.37 ka and 9.91 ± 0.58 ka. The final event occurred after deposition of unit F and before deposition of unit G. Hence, we collected OSL sample from the unit G (sample number ÇPA-6) representing the upper boundary of the first event, which yielded a date of 3.29 ± 0.14 ka and from the unit F (sample number ÇPA-3) representing the lower boundary of the first event, which yielded a date of 9.39 ± 0.37 ka (Figure 7).

4.1.3. Trench 3

Trench 3 was excavated on the eastern segment of MFZ, and it was nearly 27 m long, 3.5m wide, and 4 m deep. The trench walls clearly show eleven different units with recent soil. Brecciated limestone, which is belonging to the hanging wall unit of the NE trending fault, forms the basement unit (unit A) of the trench. This unit comprises of well strengthened unsorted limestone in various sizes in a light brown breccia. The basement unit is overlain by dark brown colored limestone blocky gravel (unit B) and reddish-brown, medium sorted muddy sandy gravel (unit C). The observable vertical displacement is more than 1.5 m in between 17 m and 19 m of trench walls. Overlying unit D consists of dark reddish-brown, unsorted limestone gravelly muddy gravel. Nearly 2 m of the vertical displacement is observed in between 4m and 6 m of trench walls. These units are overlain by yellowish-beige organic and pottery-rich clayey gravel (unit E) and dark brown, unsorted, coarse gravel (unit F). The observable vertical displacement is more than 3.5 m in between –5 m and –1 m of trench walls. Overlying unit G consists of greenish-brown gravelly sandy mud, which is belonging to crack fills. Overlying unit H consists of dark to orange, brown, well-sorted, upward fining muddy sandy gravel. Dark greenish brown organic-rich clayey silty mud represents unit I, and greyish-dark brown, poorly sorted silty clayey gravel of unit J, respectively. In addition, unit J is colluvial wedge after the final event. All these units are overlain unconformably by light to dark brown surface soil with silty clayey mud (unit K) (Figure 8).

To constrain the timing of earthquakes, a total of six OSL samples and one radiocarbon sample were collected from Trench 3. The calculated dates are consistent with both stratigraphic orders in the trench walls. The derived ages of the samples from trench 3 was dated between 2.17 ± 0.20 ka and 6.67 ± 0.35 ka (Table 3). Also, the radiocarbon sample yielded 175 ± 30BP. Further, the calibrated date for the radiocarbon sample was between 1725 calAD and 1815 calAD with a 95.4% probability (Table 4).

Based on the sedimentological, micro-stratigraphy evidence and results of dated samples, and the analysis of structural elements, four events were identified in trench 3. The earliest event occurred after deposition of unit C and before deposition of unit D. Hence, we collected OSL sample from the unit D (sample number YH-2) representing the upper boundary of the first event, which yielded a date of 6.21 ± 1.05 ka and from unit C (sample number YH-3) representing the lower boundary of the first event, which yielded a date of 6.67 ± 0.35 ka. The second event occurred after deposition of unit E and before deposition of unit F. Thus, the samples collected from the unit E yielded an OSL date of 6.18 ± 0.30 ka (YH-6) representing the lower boundary of the second event, while the samples collected from the overlying unit (unit F, YH-7) yielded a date between 4.42 ± 0.46 ka. The penultimate event occurred after deposition of unit H and before deposition of unit I. So, the samples collected from unit H yielded an OSL date of 2.17 ± 0.20 ka (YH-4) representing the lower boundary of the second event while the samples collected from the overlying unit (unit I, RC-YH-1) yielded 175 ± 30 BP. The final event occurred after the deposition of unit I and before deposition unit J Unfortunately, we could not find sufficient samples to date of upper the units J and K. On the other hand, this event must be occurred before the 175 ± 30 BP according to the radiocarbon date of the lower unit (unit I) (Figure 8).

4.1.4. Trench 4

Trench 4 was excavated on the eastern segment of MFZ, and it was nearly 13 m long, 3.5 m wide, and 3 m deep. Both trench walls have exposed nine units with recent soil cover. The basement unit (unit A) consists of a greenish dark grayish brown, deformed, and chaotic matrix, alternating with sandstone and mudstone. Overlying unit B represents brown, medium strengthened sandstone blocky gravelly sand. Unit A and Unit B are overlain unconformably by brownish grey, poor sorted, blocky gravelly sandy mud (Unit C), brownish beige gravelly muddy sand (Unit D), yellowish reddish-brown pottery rich gravelly clayey mud (Unit E), yellowish reddish-brown clayey mud (Unit F), reddish grey, brown muddy sand with pottery (Unit G), reddish brownish medium strengthened gravely mud (Unit H) and finally, the unit I is characterized by beige gravelly recent soil cover. The observable vertical displacement for Unit B and Unit G is 1 m in between 0 m and 2 m of trench walls (Figure 9).

We collected a total of four OSL samples from the walls of trench 4 to constrain the timing of earthquakes. The calculated dates are consistent with both stratigraphic orders in the trench walls. The derived dates of the samples from trench 4 were dated between 1.25 ± 0.12 ka and 11.01 ± 0.83 ka (Table 3).

Evaluation of Faulting Events

Based on the sedimentological, micro-stratigraphy evidence and results of dated samples and the analysis of structural elements, two events were identified in trench 4. The first event occurred after deposition of unit E and before deposition of unit F. Unfortunately, we did not gain certain age from Unit E and unit F due to a lack of quartz.

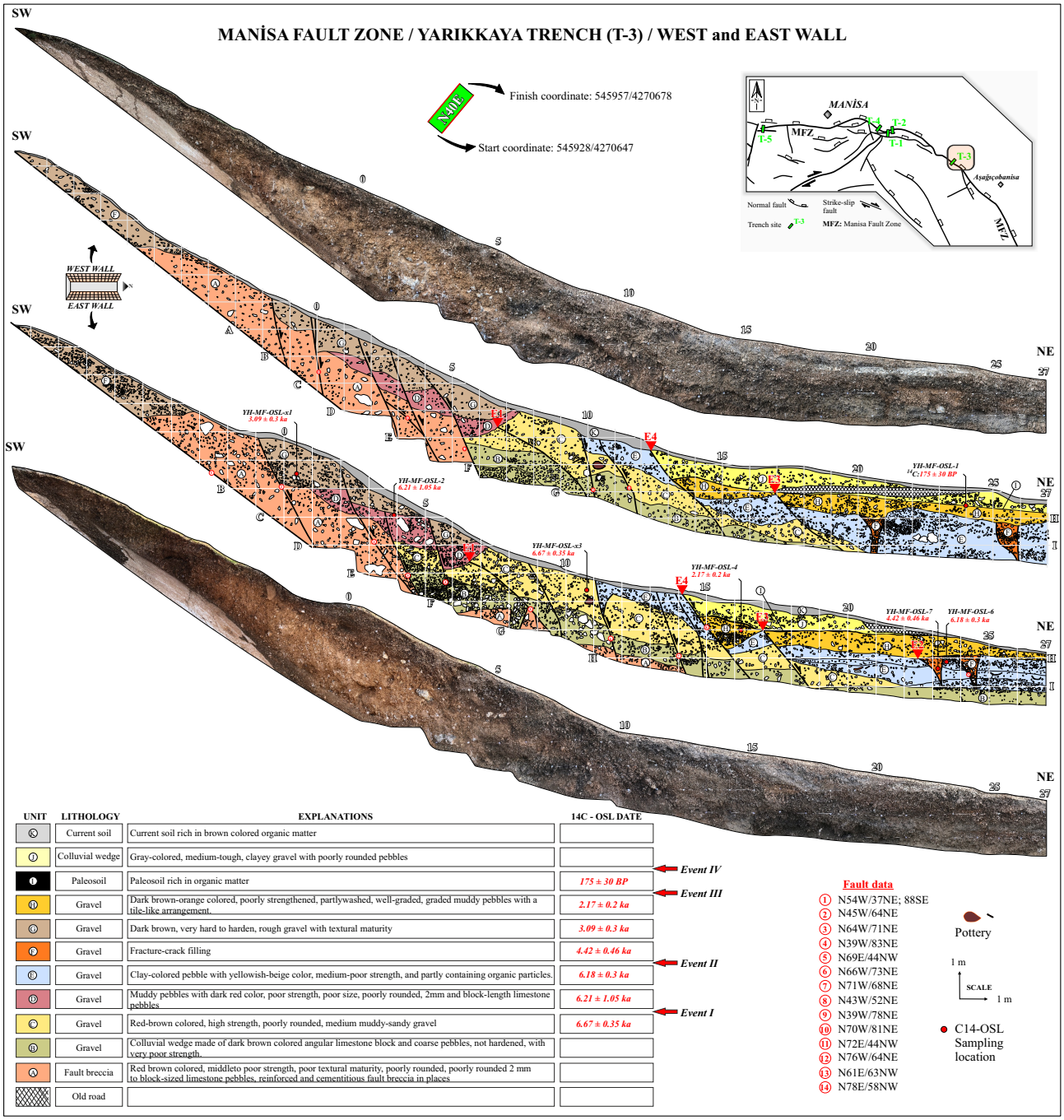


Figure 8. Photomosaic and paleoseismological log of the trench 3. See explanation in text. Red dotted circles indicate OSL dating sample locations (The east wall is flipped).

Table 4. Radiocarbon ages calculated from charcoal samples collected from the trench 3 at MFZ.

Trench name	Sample no	Coordinate (Decimal Degrees)	Age (BP)	2 sigma calibration (cal AD)
3	RC-YH-1	38.5852^{O}–27.5276^{O}	175 ± 30	1725–1815

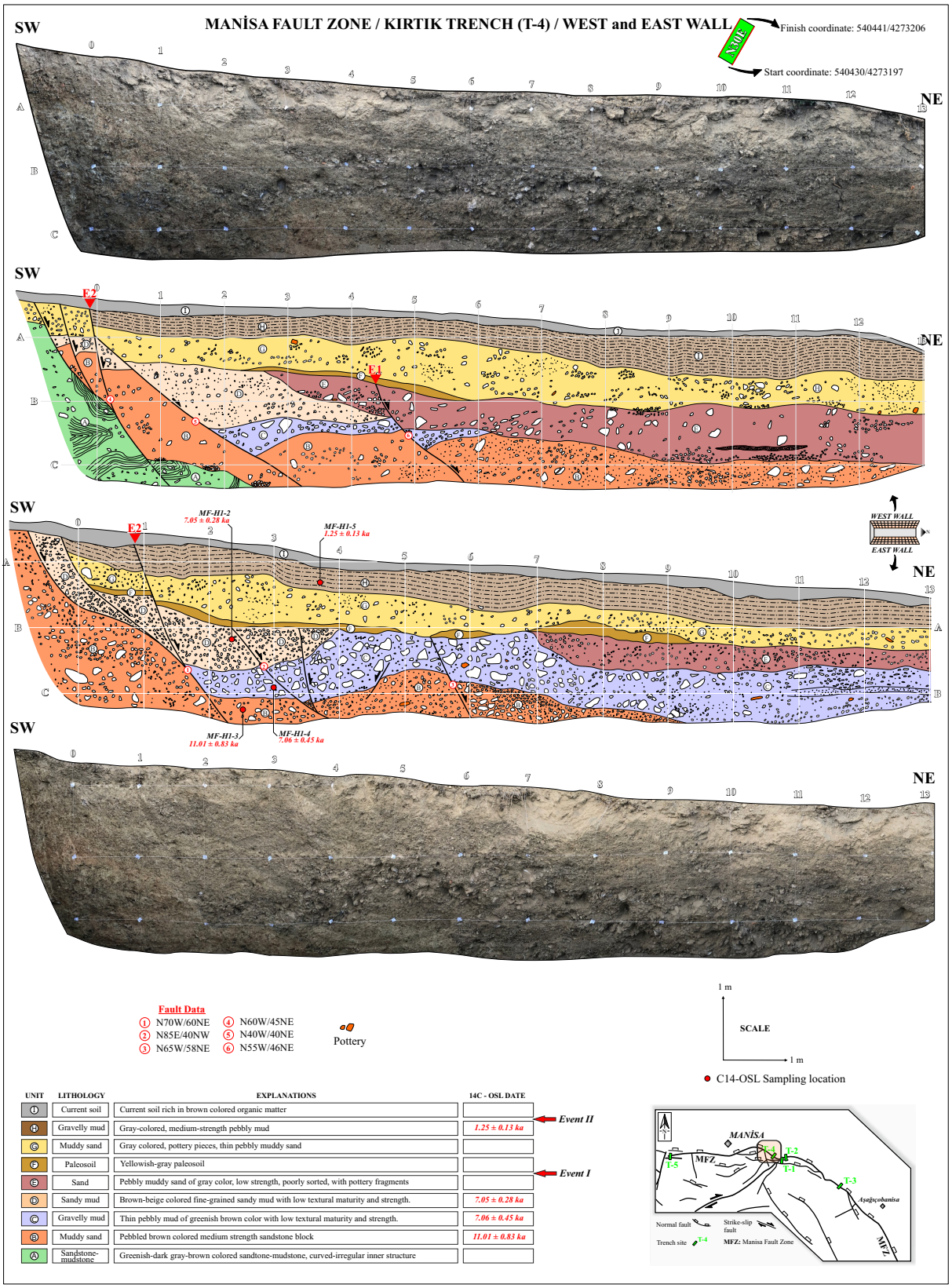


Figure 9. Photomosaic and paleoseismological log of the trench 4. See explanation in text. Red dotted circles indicate OSL dating sample locations (The east wall is flipped).

Instead of it, we dated Unit H and unit D to constrain the upper boundary and the lower boundary of the first event. The obtained OSL dates were yielded 7.05 ± 0.28 ka, and 1.25 ± 0.13 ka, respectively. The final event occurred after the deposition of unit H. Unfortunately, we could not find sufficient samples to date of upper the units I. On the other hand, this event must be occurred before the 1.25 ± 0.13 ka according to the OSL date of the lower unit (unit H) (Figure 9).

4.1.5. Trench 5

Trench 5 was excavated on the western segment of MFZ, and it was nearly 38 m long, 3.5 m wide, and deep. Both trench walls have exposed twenty-two units with recent soil cover. The basement units (unit A) consist of dark green, poorly to moderate sorted, deformed, and chaotic matrix, lenses alternating with sandstone and mudstone, greenish grey, poorly sorted, lower to moderate strengthened quartzite gravels alternating with sandstone and mudstone (unit A1), greenish grey, poorly sorted, lower to moderate strengthened and alternating with sandstone and mudstone (unit A2). Overlying units represent dark brown, lower strengthened, organic-rich levels claystone (Unit B0), brown, poorly sorted, lower strengthened angular gravelly sandy claystone (Unit B), milky brown, poorly sorted, moderate strengthened cemented sandstone gravelly sandy claystone (Unit B1), yellowish-brown, poorly sorted, moderate strengthened cemented sandstone gravelly sandy claystone (Unit B2), milky brown and yellowish-brown, poorly sorted, moderate strengthened cemented, sandy claystone (Unit B3). All of Unit A and Unit B are overlain unconformably by greenish-grey, poor sorted, lower to moderate strengthened well-folded clay (Unit C), greyish beige, lower to moderate strengthened, sandstone lenses, sandy clay (Unit C1), reddish-brown, green, and brown, lower to moderate strengthened, poorly cemented, clay with fossil fragments (Unit C2), grey, lower to moderate strengthened, altered whitish clay nodules (Unit C3), dark brown, lower to moderate strengthened, macrofossil fragment rich, folded silty clay (Unit D), greenish grey, lower strengthened sandstone lenses, sandy clay (Unit D1).

These units are overlain by yellowish-beige, poorly sorted, lower to moderate strengthened and well-cemented sandstone (Unit D2), greenish grey, lower strengthened, poorly sorted sandstone and mudstone derived from unit A1 and A2 (Unit E), orange, moderate cemented, and strengthened sand (Unit E1), greenish grey, lower strengthened, poorly cemented sandy gravel (Unit E2). Overlying unit F consists of dark brown, poorly cemented, lower strengthened gravelly sandy mud, which is belonging to a colluvial wedge. Overlying unit G0 consist of light brown sandy mud with an organic rich level. Overlying unit G consists of dark brown, gravelly sandy organic-rich mud, which is belonging to a colluvial wedge. All these units are overlain unconformably by light to dark brown surface soil with organic-rich silty clayey mud (Unit H) (Figure 10).

To constrain the timing of earthquakes, a total of four OSL samples were collected from trench 5. The calculated dates are consistent with both stratigraphic orders in the trench walls. The derived dates of the samples from trench 5 were dated between 0.67 ± 0.17 ka and 9.61 ± 0.54 ka (Table 3).

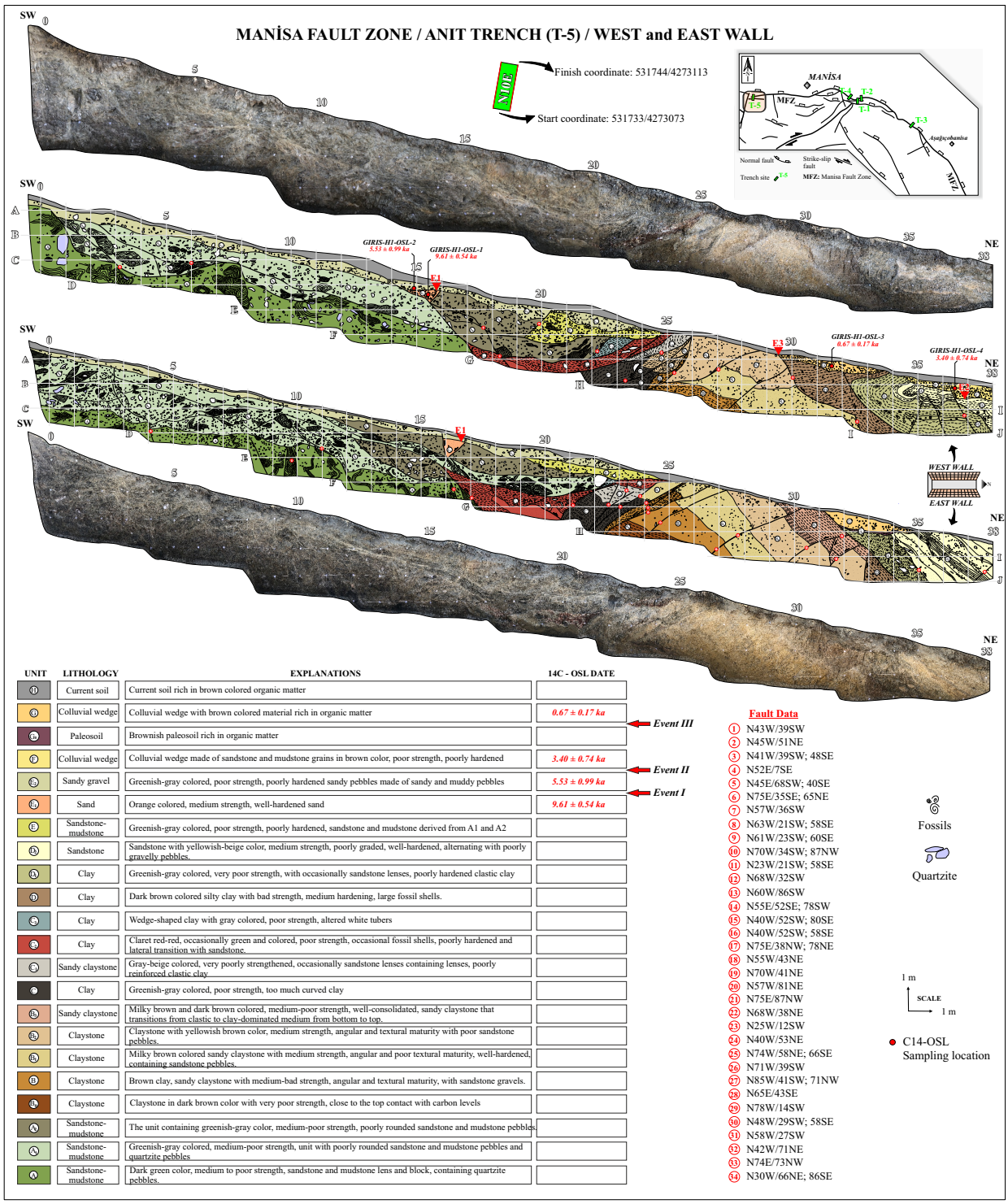
Based on the sedimentological, micro-stratigraphy evidence and results of dated samples, and the analysis of structural elements, three events were identified in trench 5. The first event occurred after deposition of unit E1 and before deposition of unit E2. Hence, we collected OSL sample from the unit E2 (sample number GR-2) representing the upper boundary of the first event, which yielded a date of 5.53 ± 0.99 ka, and from the unit E1 (sample number GR-1) representing the lower boundary of the first event, which yielded a date of 9.61 ± 0.54 ka. The second event took place before the deposition of unit F and after the deposition of unit E2. We collected both OSL samples from unit F (GR-4) and unit E2 (GR-2). The obtained OSL ages were yielded 3.40 ± 0.74 ka, and 5.53 ± 0.99 ka, respectively. The final event occurred after deposition of unit G0 and before deposition of unit G. Unfortunately, no datable material was found in Unit G0. So, for defining the lower boundary of the final event, we collected the GR-4 sample from the unit F yielded a date of 3.40 ± 0.74 ka. The date result of unit G (GR-3; 0.67 ± 0.17 ka) gives the upper boundary of the final event in trench 5 (Figure 10).

5. Discussion and Conclusion

The E-W to NW-SE-striking Manisa Fault Zone (MFZ) is one of the sources of the significant earthquakes of the Aegean region; it delimits the southern of the Manisa Basin. The zone is made up of two main fault segments, and it is an active structure with distinctly observable north dipping fault scarps. To shed light on (i) Holocene-Quaternary paleoseismic activity of MFZ, (ii) the earthquake recurrence interval and elapse time since the last activity of fault, five trenches were excavated on the eastern and the western segments. Based on this research, the following assessments and discussions can be made.

Detailed studies of trench walls and dating studies signify that MFZ is responsible for at least four surface faulting earthquakes during the Holocene. All trenches were evaluated into the Oxcal program to generate events interval using the Bayesian methods. According to the plot, trenches excavated on the eastern segment (trench 1) of MFZ provide evidence for two events after 10.65 ± 1.41 ka. Paleoseismological evidence in trench 1 suggests that the first event took place sometime between 10.65 ± 1.41ka

and 6.56 ± 0.55 ka. Moreover, the final event took place interval the 6.56 ± 0.55 ka and 0.67 ± 0.49 ka (Figure 11). Albeit, the E1 event has not been attributed to the exact earthquake due to the limited time interval of historical earthquake catalogs and lower-upper age boundary and its uncertainties, E2 corresponded with 17 AD or 926 AD earthquakes considering historical records (Table 5). Further, more than 2.5 m vertical displacements observed



UNIT	LITHOLOGY	EXPLANATIONS	14C - OSL DATE
U	Current soil	Current soil rich in brown colored organic matter	
O	Colluvial wedge	Colluvial wedge with brown colored material rich in organic matter	0.67 ± 0.17 ka
S	Paleosoil	Brownish paleosoil rich in organic matter	
P	Colluvial wedge	Colluvial wedge made of sandstone and mudstone grains in brown color, poor strength, poorly hardened	3.40 ± 0.74 ka
Sg	Sandy gravel	Greenish-gray colored, poor strength, poorly hardened sandy pebbles made of sandy and muddy pebbles	5.53 ± 0.99 ka
Sn	Sand	Orange colored, medium strength, well-hardened sand	9.61 ± 0.54 ka
E	Sandstone-mudstone	Greenish-gray colored, poor strength, poorly hardened, sandstone and mudstone derived from A1 and A2	
Sh	Sandstone	Sandstone with yellowish-beige color, medium strength, poorly graded, well-hardened, alternating with poorly gravelly pebbles.	
Ah	Clay	Greenish-gray colored, very poor strength, with occasionally sandstone lenses, poorly hardened clastic clay	
D	Clay	Dark brown colored silty clay with bad strength, medium hardening, large fossil shells.	
Cm	Clay	Wedge-shaped clay with gray colored, poor strength, altered white tubers	
Cl	Clay	Claret red-red, occasionally green and colored, poor strength, occasional fossil shells, poorly hardened and lateral transition with sandstone.	
Cs	Sandy claystone	Gray-beige colored, very poorly strengthened, occasionally sandstone lenses containing lenses, poorly reinforced clastic clay	
C	Clay	Greenish-gray colored, poor strength, too much curved clay	
Ms	Sandy claystone	Milky brown and dark brown colored, medium-poor strength, well-consolidated, sandy claystone that transitions from clastic to clay-dominated medium from bottom to top.	
Mc	Claystone	Claystone with yellowish brown color, medium strength, angular and textural maturity with poor sandstone pebbles.	
Mh	Claystone	Milky brown colored sandy claystone with medium strength, angular and poor textural maturity, well-hardened, containing sandstone pebbles.	
B	Claystone	Brown clay, sandy claystone with medium-bad strength, angular and textural maturity, with sandstone gravels.	
Mk	Claystone	Claystone in dark brown color with very poor strength, close to the top contact with carbon levels	
A	Sandstone-mudstone	The unit containing greenish-gray color, medium-poor strength, poorly rounded sandstone and mudstone pebbles	
A	Sandstone-mudstone	Greenish-gray colored, medium-poor strength, unit with poorly rounded sandstone and mudstone pebbles and quartzite pebbles	
A	Sandstone-mudstone	Dark green color, medium to poor strength, sandstone and mudstone lens and block, containing quartzite pebbles.	

Figure 10. Photomosaic and paleoseismological log of the trench 5. See explanation in text. Red dotted circles indicate OSL dating sample locations (The east wall is flipped).

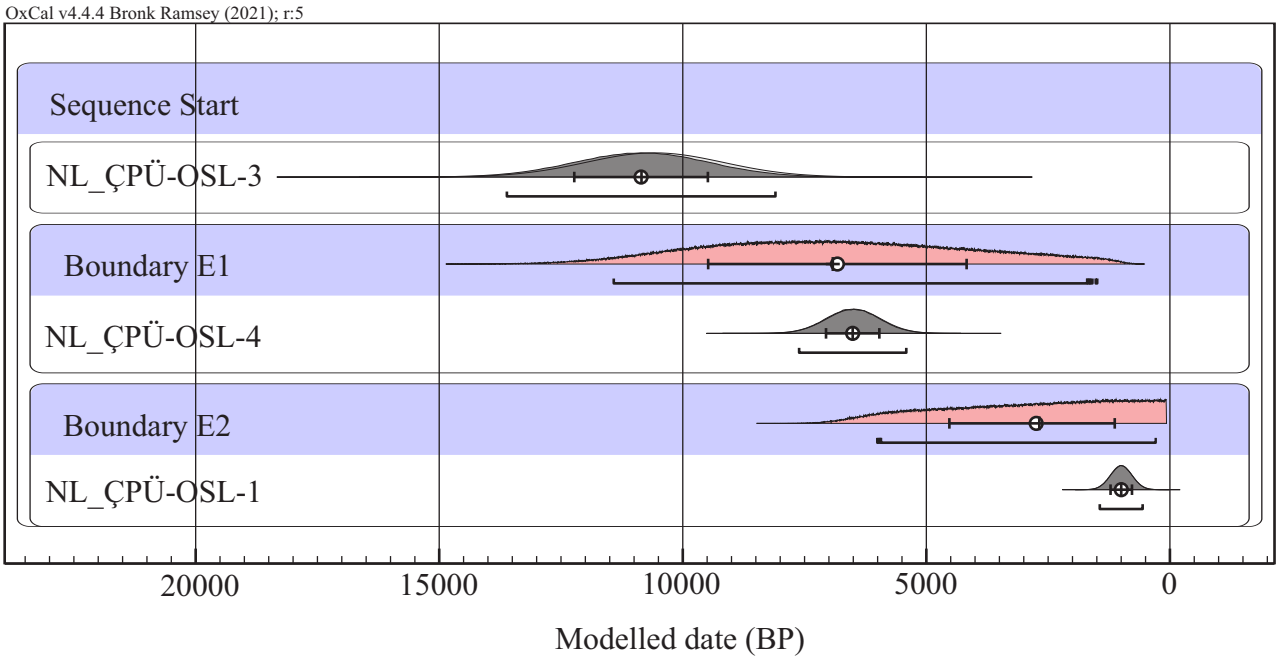


Figure 11. Preferred model from OxCal v4.4.4 (Ramsey, 2008, 2009; Reimer et al., 2009) of timing constraints on earthquakes (E1-E2) at the trench 1 on the Manisa fault zone. Ages listed in sequence are in stratigraphic order, without depth constraints.

on the fault, which are responsible for at least two events during the Quaternary period, were considered.

Paleoseismic studies in trench 2 on the eastern segment of MFZ indicate that the segment is responsible for three events after 44.63 ± 2.44 ka (Figure 12). Detailed paleoseismological evidence in trench 2 suggests that while the three events were observed in this trench, unfortunately, no historical earthquakes were recorded due to the catalog's time interval is limited (Table 5). According to the observed more than 3 m vertical displacements on the faults, this offset is believed to generate at least two or three historical earthquakes that being surface rupture in Pleistocene.

Trench data from trench 3 on the eastern segment of the MFZ, provide evidence for four events after 6.67 ± 0.35 ka (Figure 13). Detailed paleoseismological evidence in trench 3 suggests that the penultimate event took place sometime between 2.1 7 ± 0.2 ka and 175 ± 30 BP, which can be correlated with the 926 AD earthquake considering historical records. The last event observed in this trench on the eastern segment of MFZ best fits with the 1862 AD earthquakes. Moreover, E1 and E2 events have not attributed to the exact earthquake due to the limited time interval of historical earthquake catalogs (Table 5). Considering the observed more than 3.5 m vertical displacements on the fault, this offset may contain at least two earthquakes in Holocene.

Trench data from trench 4 on the eastern segment of the MFZ, provide evidence for two events after 7.05 ± 0.28 ka (Figure 14). Detail paleoseismological evidence in trench 4 suggests that the penultimate event took place sometime between 7.05 ± 0.56 ka and 1.25 ± 0.12 ka, which can be correlated with the 17 AD earthquake considering historical records. The last event observed in this trench on the eastern segment of MFZ best fit with the 926 AD earthquakes (Table 5). The first event has not correlated with the catalogs due to the limited time interval. Moreover, the observed 1 m vertical displacement, which may contain at least two events during the Holocene.

Trench data from trench 5 on the western segment of the MFZ, provide evidence for three events after 9.61 ± 0.54 ka. The first event observed in the trench, there is no record of any large earthquake in the Manisa region between 9.61 ± 0.54 ka and 5.53 ± 0.99 ka (Figure 15). The penultimate and last event observed in this trench on the western segment of MFZ best fit with the 17 AD and 926 AD earthquakes, respectively (Table 5).

Based on the well-constrained earthquake events within the five trenches we assumed that six earthquake cycles have occurred at 30.6 ± 8.8 ka (E1), 15.0 ± 5.0 ka (E2), 6.6 ± 1.3 ka (E3), 2.9 ± 1.3 ka (E4), 0.8 ± 0.4 ka (E5), and 0.1 ± 0.1 ka (E6) (Figure 16), yields average interevent times of 15.6 kyr between E1 and E2, 8.4 kyr between E2 and E3, 3.7 kyr between E3 and E4, 2.1 kyr between E4 and E5, and lastly, 0.7 kyr between E5 and E6. Moreover, considering the error parameter of ages, the interevent times could up to 29.4 kyr. While these values yield a closed holistically the recurrence interval ranging

Table 5. Event timing in T1, T2, T3, T4 and T5 trenches along the MFZ and corresponding earthquakes.

Trench1-Event	%95.4-2 sigma-modelled with Oxcal range from - to	C_Earthquakes
E1	7552 BC–2336 BC	-
E2	2289 BC– 1491 AD	**17 AD, 926 AD**
Trench2-Event		
E1	37365 BC–19083 BC	-
E2	17579 BC–6327 BC	-
E3	5442 BC–1476 BC	–
Trench3-Event		
E1	4378 BC–2844 BC	-
E2	3440 BC–810 BC	-
E3	468 AD–1618 AD	**926 AD**
E4	1860 AD–2007 AD	**1862 AD**
Trench4-Event		
E1	3713 BC–71 AD	**17 AD**
E2	983 AD–1417 AD	**926 AD**
Trench5-Event		
E1	6552 BC–3040 BC	-
E2	2650 BC–166 AD	**17 AD**
E3	800 AD–1772 AD	**926 AD**

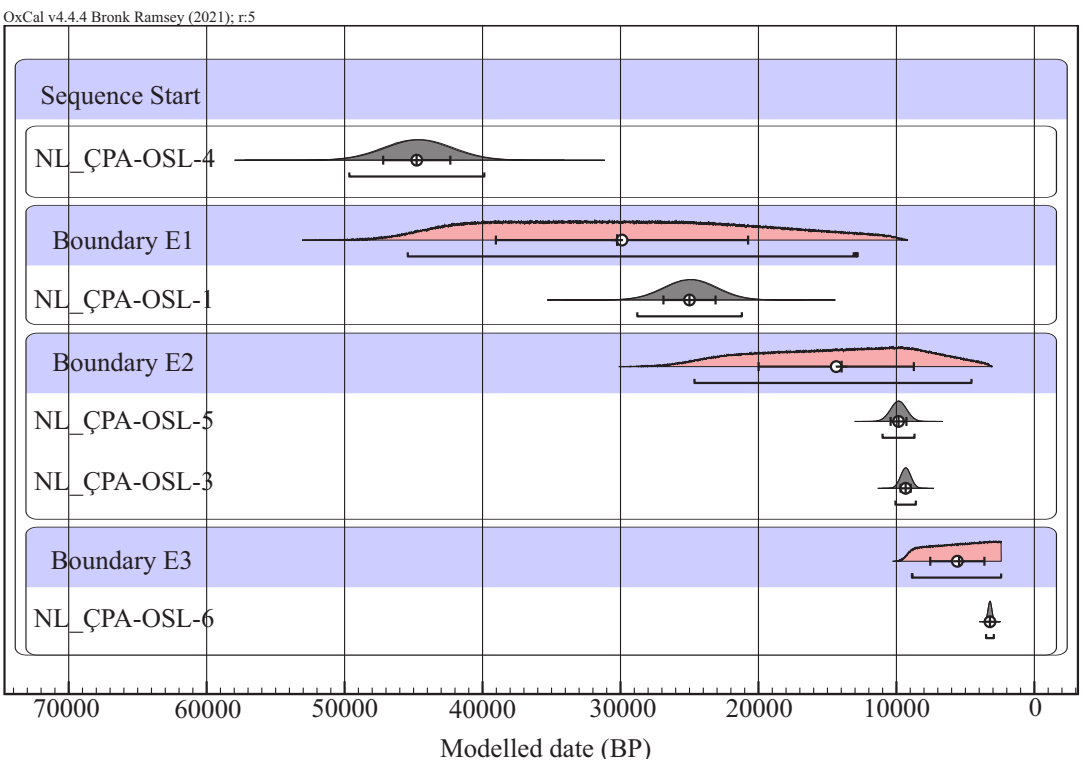


Figure 12. Preferred model from OxCal v4.4.2 (Ramsey, 2008, 2009; Reimer et al., 2009) of timing constraints on earthquakes (E1-E3) at the trench 2 on the Manisa fault zone. Ages listed in sequence are in stratigraphic order, without depth constraints.

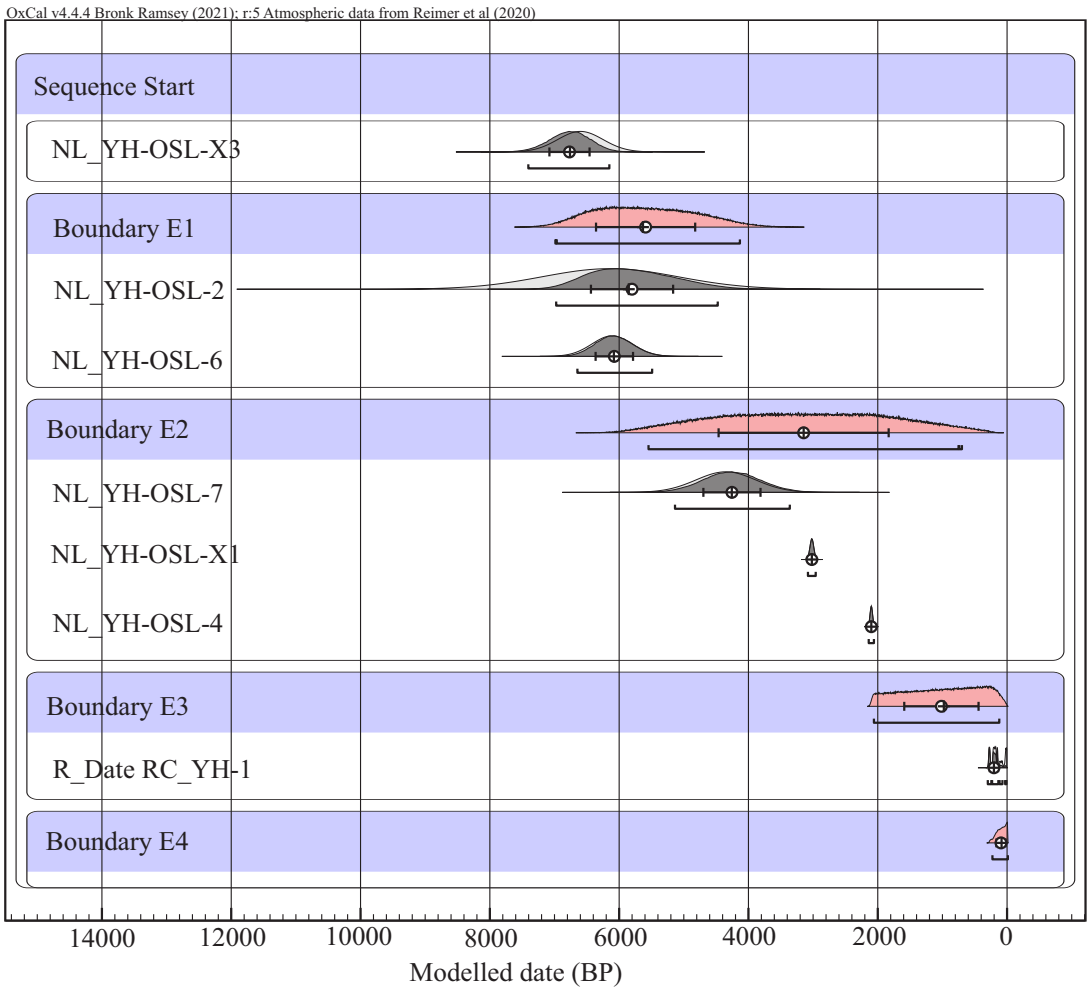


Figure 13. Preferred model from OxCal v4.4.4 (Ramsey, 2008, 2009; Reimer et al., 2009) of timing constraints on earthquakes (E1-E4) at the trench 3 on the Manisa fault zone. Ages listed in sequence are in stratigraphic order, without depth constraints.

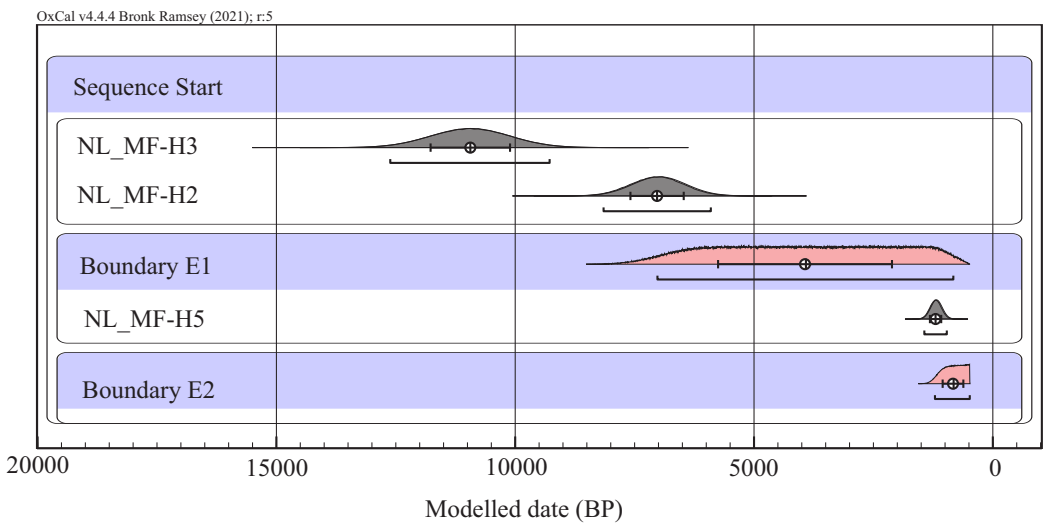


Figure 14. Preferred model from OxCal v4.4.4 (Ramsey, 2008, 2009; Reimer et al., 2009) of timing constraints on earthquakes (E1-E2) at the trench 4 on the Manisa fault zone. Ages listed in sequence are in stratigraphic order, without depth constraints.

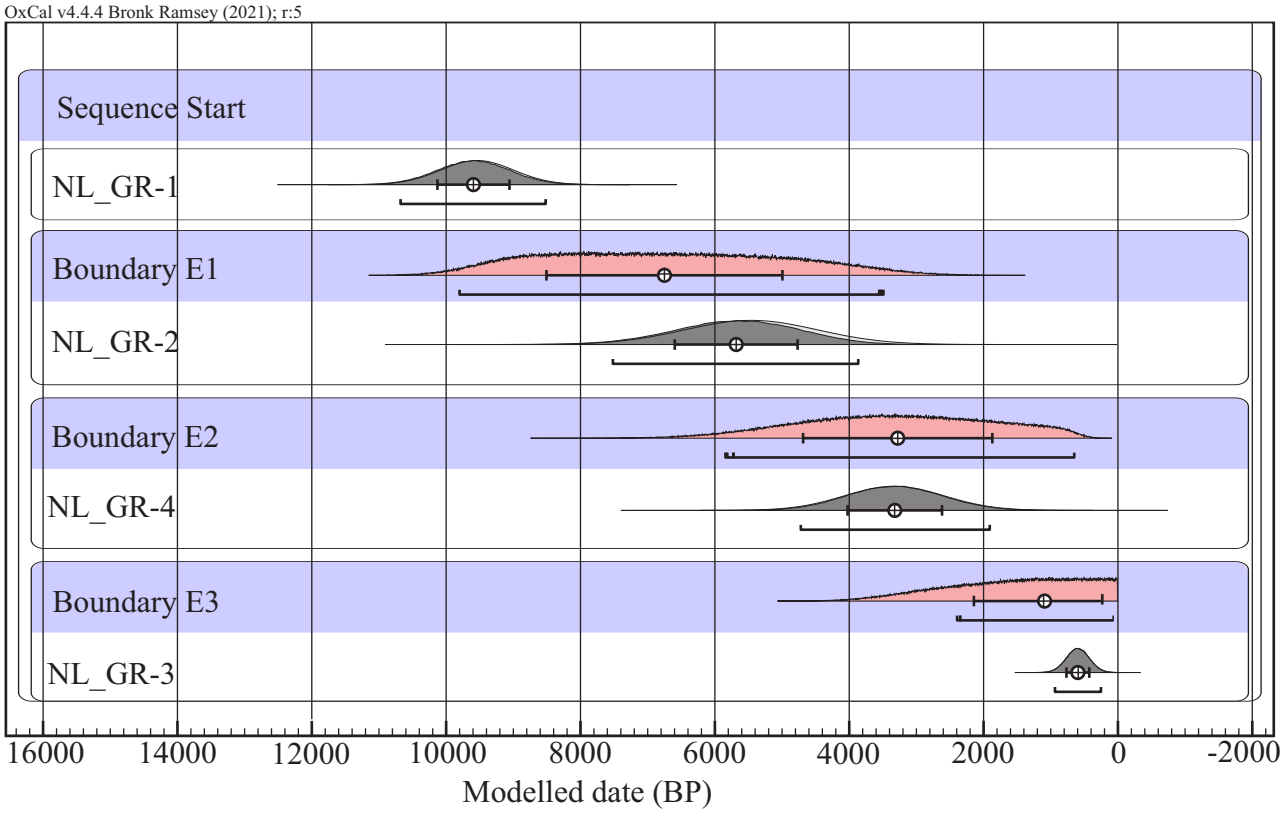


Figure 15. Preferred model from OxCal v4.4.2 (Ramsey, 2008, 2009; Reimer et al., 2009) of timing constraints on earthquakes (E1-E3) at the trench 5 on the Manisa fault zone. Ages listed in sequence are in stratigraphic order, without depth constraints.

Table 6. Earthquake timing, interevent time, and recurrences interval in the eastern segment of Manisa Fault Zone.

E[a]	Dates A (ka)			Interevent Time I (kyr) (AE_{first}-AE_{second})			Recurrences Interval[b] R (kyr)								
	A_{min}	$A_{average}$	A_{max}	I_{min} (AE_{min}-AE_{max})	$I_{average}$ ($AE_{average}$-$AE_{average}$)	I_{max} (AE_{max}-AE_{min})	$R_{Holocene}$			$R_{Pleistocene}$			$R_{Holistically}$		
							R_{min}	$R_{average}$	R_{max}	R_{min}	$R_{average}$	R_{max}	R_{min}	$R_{average}$	R_{max}
E1	21.8[P]	30.6[P]	39.4[P]												
E2	10.0[H]	15.0[P]	20.0[P]	1.8[PE]	15.6[PE]	29.5[PE]									
E3	5.3[H]	6.6[H]	7.9[H]	2.1[HE]	8.4[PE]	14.7[PE]									
E4	1.6[H]	2.9[H]	4.2[H]	1.1[HE]	3.7[HE]	6.3[HE]	0.95	2.2	3.8	1.8	12.0	22.1	1.1	6.12	11.1
E5	0.4[H]	0.8[H]	1.2[H]	0.4[HE]	2.1[HE]	3.8[HE]									
E6	0[H]	0.1[H]	0.2[H]	0.2[HE]	0.7[HE]	1.2[HE]									

[a]: According to preferred model derived from Oxcal (Ramsey, 2008, 2009; Reimer et al., 2009).
[b]*: Represents recurrences interval based on the formula.
The formula:
R_{min}: ($AE1_{min}$-$AE2_{max}$) +($AE2_{min}$-$AE3_{max}$) +($AE3_{min}$-$AE4_{max}$)/n-1
$R_{average}$: ($AE1_{average}$-$AE2_{average}$) +($AE2_{average}$-$AE3_{average}$) +($AE3_{average}$-$AE4_{average}$)/n-1
R_{max}: ($AE1_{max}$-$AE2_{min}$) +($AE2_{max}$-$AE3_{min}$) +($AE3_{max}$-$AE4_{min}$)/n-1
E: Events, N: number of events, H: Holocene, P: Pleistocene, HE: Holocene Event, PE: Pleistocene Event.

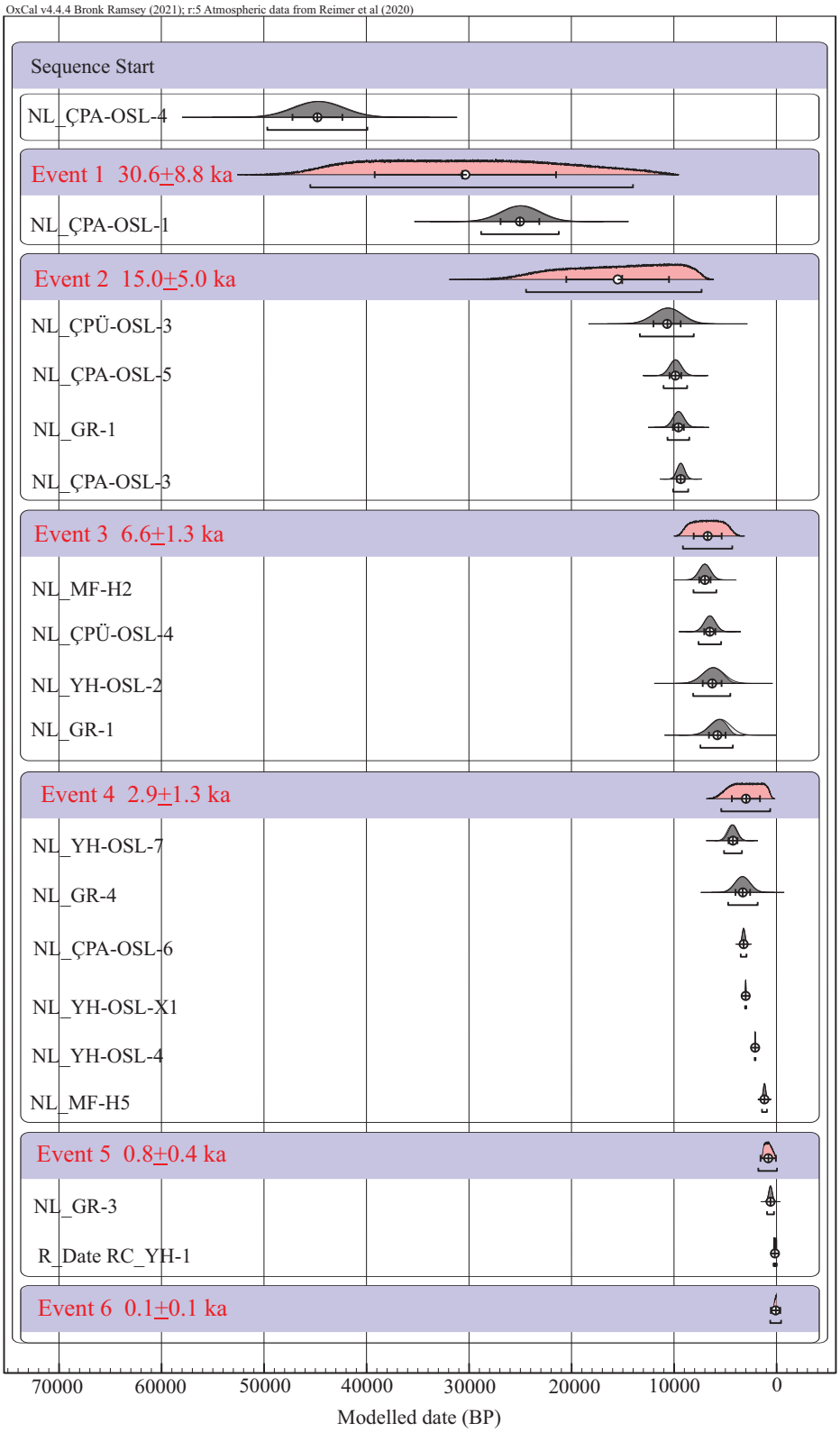


Figure 16. Preferred model from OxCal v4.4.4 (Ramsey, 2008, 2009; Reimer et al., 2009) of timing constraints on earthquakes (E1-E6) at T1-T5 trenches on the Manisa fault zone. Ages listed in sequence are in stratigraphic order, without depth constraints. Prior probability distribution function (Pdf) ages are defined by the calibrated radiocarbon and OSL ages. Posterior Pdf ages are calculated from the Bayesian OxCal analysis.

Table 7. A comparison of trench-based paleoseismological studies on normal fault in Western Anatolia. Fault lengths and Mmax adapted from Emre et al. (2018). [a]. A capable of maximum earthquake magnitude (Emre et al ., 2018). ns: non systematic.

Fault -Segment Name	Length (km)	Mmax[a]	Slip rate (mm)	Recurrence Interval (year)	C_Earthquakes
1. Edremit FZ-Küçükkuyu Seg.	23	6.66	-	-ns	*160/253 AD *1944 AD (M6,8)
2. BMGS İncirliova Seg.	31	6.83	1.76	250-1900	-
3. BMGS Umurlu Seg.	25	6.71	1.39		*1899 AD *1653 AD
4. BMGS Atça Seg.	34	6.88	1.14		*238/244/262 AD
5. BMGS Pamukören Seg.	26	6.73	0.96		-
6. Yatağan F.	17	6.48	0.2	-	*142 AD
7. Muğla F.	25	6.71	-	-	-
8. Izmir F.	38	7.12	-	-	*1688 AD
9. Dinar F.	55	6.77	0.37–0.56	523	-
10. Dinar F.	55	6.77	1	1500–2000	-
11. Erdogmus F.	12	6.3	-	910	-
12. Bolvadin F.	7	5.98	0.63–0.1	-	94-530 AD
13. Manisa F. West Seg.	45	6.9	0.3	-	926-1595/1664-1845 AD
14. Manisa F. East Seg.	45	6.9	0.1–1	950–3800	17-926-1862 AD

1: Sözbilir et al. (2016). 2-3-4-5: Altunel et al. (2009). 6: Basmenji et al. (2021). 7: Akyüz et al. (2021). 8: Tepe et al. (2021b). 9: Kürçer et al. (2021). 10: Altunel et al. (1999). 11: Gürboğa (2013). 12: Özkaymak et al (2019). 13: Özkaymak et al (2013). 14: This study.

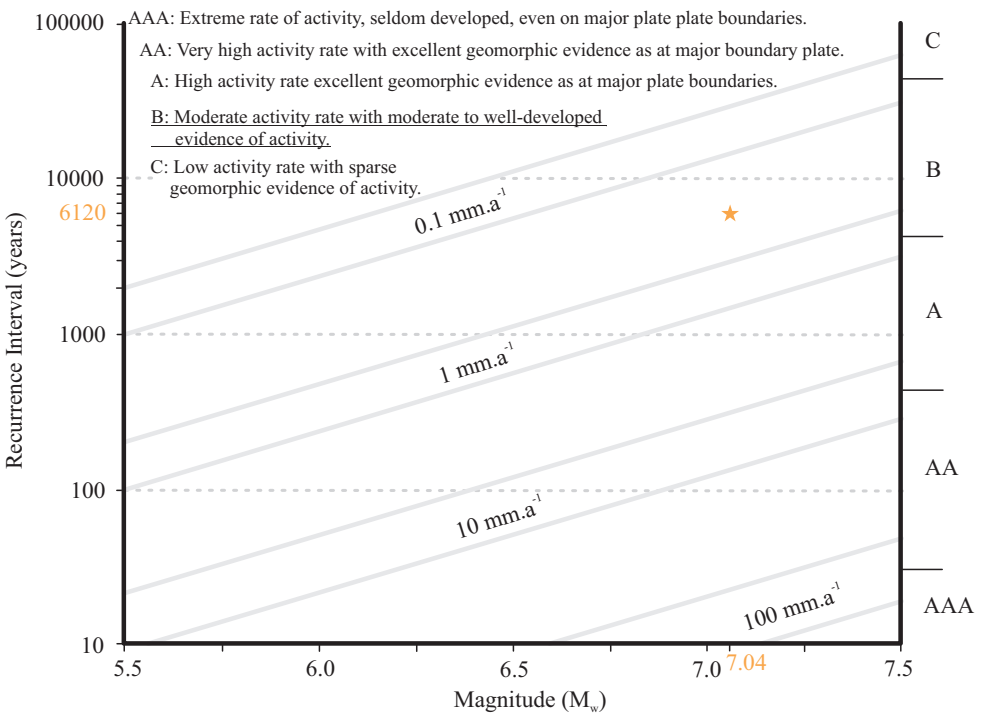


Figure 17. Average earthquake recurrence interval versus earthquake magnitude and annual slip rate of active faults (modified from Slemmons and de Polo, 1986).

from 0.95 kyr to 3.8 kyr for Holocene, 1.8 kyr to 22.1 kyr for Pleistocene (Table 6). This result shows variable and not consistent recurrences intervals for MFZ. The inconsistency and variable recurrences interval are also reported in many active faults worldwide (e.g., Biasi et al. 2002; Sözbilir et al., 2016; Üner et al., 2019; Kürçer et al., 2019, Mozafari et al, 2019). In addition to that, a remarkable number of paleoseismological studies which were conducted on normal faults in western Anatolia (Altunel et al., 1999; Gürboğa, 2013; Özkaymak et al., 2013,2019; Sözbilir et al., 2016; Basmenji et al., 2021; Akyüz et al., 2021; Kürçer et al., 2021). From these studies, the earthquake recurrence interval was only estimated for Edremit Fault Zone (non-systematic) (Sözbilir et al., 2016), Büyük Menderes Graben System (250-1900 years) (Altunel, 1999), Dinar fault (523-2000 years) (Altunel et al., 1999; Kürçer et al., 2021) and Erdoğmuş fault (910 years) (Gürboğa, 2013) (Table 7).

It was noted that MFZ could generate an earthquake up to 7.04, according to Wells and Coppersmith's (1994) empirical equations. Moreover, considering the holistically average recurrence interval, suggests that the MFZ can be categorized as class B, according to the taxonomy of Slemmons and de Polo (1986), which signifies a fault of moderate activity rate with moderate to well-developed geomorphic evidence of activity. Also, this scheme suggests that the annual long-term slip rate can be between 0.1 mm/year and 1 mm/year when the estimated earthquake and recurrence interval evaluated together (Figure 17). This slip rate value best fits with the rates calculated for dip-slip normal faults in western Anatolia, Greece, and Italy (Caputo, 1995; Caputo et al., 2004; Pavlides and Caputo, 2004; Papanikolaou et al., 2005; Özkaymak et al., 2011; Özkaymak, 2015; Tsodoulos et al., 2016; Özalp et al., 2018; Özkaymak et al., 2019) (Table 7).

Our paleoseismological trenching results are consistent with both surface-based and trench-based paleoseismological studies on the western segment of MFZ. So, besides our studies, there are limited paleoseismological studies conducted along the western segment of MFZ (Özkaymak et al., 2011 and Akçar et al., 2012). From these studies, Özkaymak et al. (2011) stated that MFZ was responsible for at least three historical earthquakes, which were possibly related to 926 AD, 1595 AD, or 1664 AD and 1845 AD. Further, Akçar et al. (2012) put forward two different paleoseismological scenarios. Their first scenario yields two seismic events, one at 13.7 ± 0.8 ka with a displacement of 0.5 ± 0.2 m and one at 7.8 ± 0.5 ka with 2.15 ± 0.35 m offset. For the second scenario, they obtained a single seismic event at 8.6 ± 0.6 ka with 2.65 ± 0.35 m of slip.

According to these findings and historical catalogs, if the 1845 AD and 1862 AD earthquake is accepted to have occurred on MFZ, it can be understood that the western segment of MFZ had broken during the 1845 AD earthquakes, then it ruptured in a way that triggers eastern segment of MFZ in 1862 AD earthquakes. On the other hand, in light of the proposed interevent time, the estimation of the recurrence interval for the MFZ varied between 0.95 ka and 3.8 ka for the Holocene. The elapsed time since the most recent surface ruptured earthquake on the MFZ is 159 years. Accordingly, MFZ poses a significant hazard; therefore, it is necessary to assess the potential seismic hazard for the densely populated area of Manisa, Western Anatolia.

Acknowledgments

This work was part of a M.Sc. Thesis undertaken by İsmail Duran at the Institute of Natural and Applied Sciences, Dokuz Eylül University, Turkey. This research was supported by Sanko Enerji Sanayi A.Ş. (DEU-Working Capital Project: JEO.DAN.18.A07). We would like to thank Manisa Governorship, Manisa Şehzadeler, and Manisa Yunusemre municipal officials and employees for their logistical contribution. Moreover, the authors would like to thank to Dr. Selim Özalp and the anonymous reviewer for their critical and constructive comments that greatly contributed to improving the final version of the paper.

References

Aitken (1998). Introduction to optical dating: the dating of Quaternary sediments by the use of photon-stimulated luminescence. Clarendon Press.

Akçar N, Tikhomirov D, Özkaymak Ç, Ivy-Ochs S, Alfimov V et al. (2012). 36Cl exposure dating of paleoearthquakes in the Eastern Mediterranean: First results from the western Anatolian Extensional Province, Manisa fault zone, Turkey. Geological Society of America Bulletin 124 (11-12): 1724-1735. doi: 10.1130/B30614.1

Aktar M, Karabulut H, Özalaybey S, Childs D (2007). A conjugate strike-slip fault system within the extensional tectonics of Western Turkey. Geophysical Journal International 171 (3): 1363-1375. doi: 10.1111/j.1365-246X.2007.03598.x

Akyol N, Karagöz Ö (2009). Empirical attenuation relationships for western Anatolia, Turkey. Turkish Journal of Earth Sciences 18 (3): 351-382. doi: 10.3906/yer-0705-2

Akyol N, Zhu L, Mitchell BJ, Sözbilir H, Kekovalı K (2006). Crustal structure and local seismicity in western Anatolia. Geophysical Journal International 166 (3): 1259-1269. doi: 10.1111/j.1365-246X.2006.03053.x

Akyüz HS, Altunel E (2001). Geological and archaeological evidence for post–Roman earthquake surface faulting at Cibyra, SW Turkey. Geodinamica Acta 14 (1-3): 95-101. doi: 10.1080/09853111.2001.11432437

Akyüz HS, Basmenji M, Kirkan E, Aksoy ME, Dikbaş, A et al. (2021). Muğla Fault, SW Turkey: New morphometric, Geomorphologic and Paleoseismologic Findings. Bulletin For Earth Sciences 42 (2): 232-260 (In Turkish) doi: 10.17824/yerbilimleri.868411

Allen CR (1974). Geological criteria for evaluating seismicity. Geological Society of America Bulletin 86: 1041-1057.

Altunel, E (1999). Geological and geomorphological observations in relation to the 20 September 1899 Menderes earthquake, western Turkey. Journal of the Geological Society 156 (2): 241-246. doi: 10.1144/gsjgs.156.2.0241

Altunel E, Barka A, Akyüz S (1999). Palaeoseismicity of the Dinar fault, SW Turkey. Terra Nova 11 (6): 297-302. doi: 10.1046/j.1365-3121.1999.00262.x

Altunel E, Meghraoui M, Karabacak V, Akyüz SH, Ferry M et al (2009). Archaeological sites (tell and road) offset by the Dead Sea Fault in the Amik Basin, southern Turkey. Geophysical Journal International 179 (3): 1313-1329. doi: 10.1111/j.1365-246X.2009.04388.x

Ambraseys NN (1988). Engineering Seismology. Earthquake Engineering and Structural Dynamics 17: 1-105.

Ambraseys N (2009). Earthquakes in the Mediterranean and Middle East: a multidisciplinary study of seismicity up to 1900. Cambridge, United Kingdom: Cambridge University Press.

Ambraseys NN, Finkel C (1995). The seismicity of Turkey and adjacent areas: a historical review, 1500-1800. İstanbul, Eren.

Ambraseys NN, Jackson JA (1998). Faulting associated with historical and recent earthquakes in the Eastern Mediterranean region. Geophysical Journal International 133 (2): 390-406. doi: 10.1046/j.1365-246X.1998.00508.x

Arpat E, Bingöl E (1969). Ege Bölgesi graben sisteminin gelişimi üzerine düşünceler. Maden Tetkik ve Arama Dergisi 73: 1-8 (In Turkish).

Barka AA (1992). The north Anatolian fault zone. In Annales tectonicae Vol. 6, No. Suppl, pp. 164-195.

Basmenji M, Akyuz HS, Kirkan E, Aksoy ME, Ucarkus G et al. (2021). Earthquake history of the Yatagan Fault (Mugla, SW Turkey): implications for regional seismic hazard assessment and paleoseismology in extensional provinces. Turkish Journal of Earth Sciences 30 (2): 161-181. doi: 10.3906/yer-2006-23

Başarır Baştürk N, Özel NM, Altınok Y, Duman TY (2017). Türkiye ve yakın çevresi için geliştirilmiş tarihsel dönem (MÖ 2000 – MS 1900) deprem Katalogu. Türkiye Sismotektonik Haritası Açıklama Kitabı, MTA Özel Yayınlar Serisi-35, 287 S. Ankara, 2016.

Bellier O, Över S, Poisson A, Andrieux J (1997). Recent temporal change in the stress state and modern stress field along the North Anatolian Fault Zone (Turkey). Geophysical Journal International 131 (1): 61-86.

Biasi GP, Weldon RJ, Fumal TE, Seitz GG (2002). Paleoseismic event dating and the conditional probability of large earthquakes on the southern San Andreas fault, California. Bulletin of the Seismological Society of America 92 (7): 2761-2781. doi: 10.1785/0120000605

Bozkurt E, Sözbilir H (2006). Evolution of the large-scale active Manisa Fault, southwest Turkey: Implications on fault development and regional tectonics. Geodinamica Acta 19 (6): 427-453.

Bozkurt E (2001). Neotectonics of Turkey – a synthesis. Geodinamica Acta 14: 3-30.

Bozkurt E (2003). Origin of NE-trending basins in western Turkey. Geodinamica acta 16 (2-6): 61-81. doi: 10.1016/S0985-3111(03)00002-0

Candan O, Dora OÖ, Oberhänsli R, Koralay E, Çetinkaplan M et al. (2011). Stratigraphy Of The Pan–African Basement Of The Menderes Massif And The Relationship With Late Neoproterozoic/Cambrian Evolution Of The Gondwana. Bulletin of the Mineral Research and Exploration 142 (142): 25-68.

Caputo R (1995). Evolution of orthogonal sets of coeval extension joints. Terra nova 7 (5): 479-490. doi: 10.1111/j.1365-3121.1995.tb00549.x

Caputo R, Helly B (2008). The use of distinct disciplines to investigate past earthquakes. Tectonophysics 453: 7-19. doi: 10.1016/j.tecto.2007.05.007

Caputo R, Helly B, Pavlides S, Papadopoulos G (2004). Palaeoseismological investigation of the Tyrnavos Fault, Central Greece. A contribution to the seismic hazard assessment of Thessaly. Tectonophysics 394 (1): 1-20. doi: 10.1016/j.tecto.2004.07.047

Dewey JF, Şengör AMC (1979). Aegean and surrounding regions: Complex multiplate and continuum tectonics in a convergent zone. GSA Bulletin 90: 84-92.

Doğan T, Cetin H, Yegingil Z, Topaksu M, Yüksel M et al. (2015). Optically stimulated luminescence dating of Holocene alluvial fans, East Anatolian Fault System, Turkey. Radiation Effects and Defects in Solids 170 (7-8): 630-644. doi: 10.1080/10420150.2015.1077333

Emre Ö, Duman TY, Özalp S, Şaroğlu F, Olgun Ş et al. (2018). Active fault database of Turkey. Bulletin of Earthquake Engineering 16 (8): 3229-3275. doi: 10.1007/s10518-016-0041-2

Ergin K, Güçlü U, Uz Z (1967). Türkiye ve civarının deprem kataloğu, milâttan sonra 11 yılından 1964 sonuna kadar. TC, İstanbul Teknik Üniversitesi, Maden Fakültesi, Arz Fiziği Enstitüsü.

Eski S, Sözbilir H, Uzel B, Özkaymak Ç, Sümer Ö (2020). Investigation of morphotectonic evolution of Gölmarmara fault using GIS-Based methods, Gediz Graben, Western Anatolia. Geological Bulletin of Turkey 63 (3): 345-372. doi: 10.25288/tjb.679584

Fattahi M, Nazari H, Bateman, MD, Meyer B et al. (2010). Refining the OSL age of the last earthquake on the Dheshir fault, Central Iran. Quaternary Geochronology 5(2-3): 286-292. doi: 10.1016/j.quageo.2009.04.005

Fattahi M, Walker RT (2007). Luminescence dating of the last earthquake of the Sabzevar thrust fault, NE Iran. Quaternary Geochronology 2 (1-4): 284-289. doi: 10.1016/j.quageo.2006.06.006

Foumelis M, Papazachos C, Papadimitriou E, Karakostas V, Ampatzidis D et al. (2021). On rapid multidisciplinary response aspects for Samos 2020 M 7.0 earthquake. Acta Geophysica 69: 1025-1048. doi: 10.1007/s11600-021-00578-6

Guidoboni E, Comastri A, Traina G (1994) Catalogue of ancient earthquakes in the Mediterranean area up to the 10th century. Rome, Italy: Ist Naz Geofis.

Gürboğa ŞD, Koçyiğit A, Ruffet G (2013). Episodic two-stage extensional evolutionary model for southwestern Anatolian graben–horst system: new field data from the Erdoğmuş-Yenigediz graben (Kütahya). Journal of Geodynamics 65: 176-198. doi: 10.1016/j.jog.2012.06.007

Hakyemez HY, Erkal T, Göktas F (1999). Late Quaternary evolution of the Gediz and Büyük menderes grabens, western Anatolia, Turkey. Quaternary Science Reviews 18 (4-5): 549-554. doi: 10.1016/S0277-3791(98)00096-1

Hancock PL, Barka AA. (1987). Kinematic indicators on active normal faults in western Turkey. Journal of Structural Geology 9 (5-6): 573-584. doi: 10.1016/0191-8141(87)90142-8

Jolivet L, Brun JP (2010). Cenozoic geodynamic evolution of the Aegean. Int. J. Earth Sci. 99: 109-138. doi: 10.1007/s00531-008-0366-4

Jolivet L, Faccenna C, Huet B, Labrousse L, Le Pourhiet L et al. (2013). Aegean tectonics: Strain localisation, slab tearing and trench retreat. Tectonophysics 597: 1-33. doi: 10.1016/j.tecto.2012.06.011

Jolivet L, Menant A, Sternai P, Rabillard A, Arbaret L et al. (2015). The geological signature of a slab tear below the Aegean. Tectonophysics 659: 166-182. doi: 10.1016/j.tecto.2015.08.004.

Ketin İ. (1968). Relations between general tectonic features and the main earthquake regions of Turkey. Bulletin of the Mineral Research and Exploration 71 (71).

Koçyiğit A, Özacar AA (2003). Extensional neotectonic regime through the NE edge of the outer Isparta Angle, SW Turkey: new field and seismic data. Turkish Journal of Earth Sciences, 12 (1): 67-90.

Koçyigit A, Yusufoglu H, Bozkurt E (1999). Discussion on evidence from the Gediz Graben for episodic two-stage extension in western Turkey. Journal of the Geological Society, London 156: 1240-1242. doi : 10.1144/gsjgs.156.6.1240

Kürçer A, Özalp S, Özdemir E, Güldoğan ÇU, Duman TY (2019). Active tectonic and paleoseismologic characteristics of the Yenice-Gönen fault, NW Turkey, in light of the 18 March 1953 Yenice-Gönen Earthquake (Ms= 7.2). Bulletin of the Mineral Research and Exploration 159: 29-62. doi: 10.19111/bulletinofmre.500553

Kürçer A, Özdemir E, Olgun Ş, Özalp S, Çan T et al. (2021). Active tectonic and paleoseismological characteristics of the Dinar Fault, SW Anatolia, Turkey. Mediterranean Geoscience Reviews 3: 219-251. doi: 10.1007/s42990-021-00052-x

McCalpin JP (2009). Application of paleoseismic data to seismic hazard assessment and neotectonic research. International Geophysics 95: 1-106. doi: 10.1016/S0074-6142(09)95009-4

Mozafari N, Sümer Ö, Tikhomirov D, Ivy-Ochs S, Alfimov V (2019). Holocene seismic activity of the Priene–Sazlı Fault revealed by cosmogenic 36Cl, Western Anatolia, Turkey. Turkish Journal of Earth Sciences 28 (3): 410-437. doi: 10.3906/yer-1810-6

Murray AS, Wintle AG (2000). Luminescence dating of quartz using an improved single-aliquot regenerative-dose protocol. Radiation measurements 32 (1): 57-73. doi: 10.1016/S1350-4487(99)00253-X

Murray AS, Wintle AG (2003). The single aliquot regenerative dose protocol: potential for improvements in reliability. Radiation measurements 37 (4-5): 377-381. doi: 10.1016/S1350-4487(03)00053-2

Oğuz M (1966). Manisa Dağının Kuzey ve Kuzeybatısının Jeolojisi (Geology of the northern and Northwestern part of the Manisa Dag), Engl. summary: Fac. Sci. Ege Univ., Sci. Rept., no. 33, 20 p., İzmir.

Okay AI, Satir M, Maluski H, Siyako M, Monié P et al. (1996). Paleo and Neo-tethyan events in Northwestern Turkey: Geologic and geochronologic constraints. In: Yin A, Harrison TM (editors). The tectonic evolution of Asia. Cambridge, UK: Cambridge Univ. Press, pp. 420-441.

Özalp S, Emre Ö, Şaroğlu F, Özaksoy V, Elmacı H et al. (2018). Active fault segmentation of the Çivril Graben System and surface rupture of the 1 October 1995 Dinar earthquake (Mw 6.2), Southwestern Anatolia, Turkey. Journal of Asian Earth Sciences 166: 136-151. doi: 10.1016/j.jseaes.2018.07.037

Özkaymak Ç (2012). Manisa Havzasi'nin Aktif Tektoniği ve Depremselliği, Batı Anadolu, Türkiye. PhD, Dokuz Eylül University, İzmir, Turkey (In Turkish).

Özkaymak Ç (2015). Tectonic analysis of the Honaz Fault (western Anatolia) using geomorphic indices and the regional implications. Geodinamica Acta 27 (2-3): 110-129. doi: 10.1080/09853111.2014.957504

Özkaymak Ç, Sözbilir H (2008). Stratigraphic and structural evidence for fault reactivation: the active Manisa fault zone, western Anatolia. Turkish Journal of Earth Sciences 17 (3): 615-635.

Özkaymak Ç, Sözbilir H (2012). Tectonic geomorphology of the Spildağı high ranges, western Anatolia. Geomorphology 173:128-140. doi: 10.1016/j.geomorph.2012.06.003

Özkaymak Ç, Sözbilir H, Gecievi MO, Tiryakioğlu, İ (2019). Late Holocene coseismic rupture and aseismic creep on the Bolvadin Fault, Afyon Akşehir Graben, western Anatolia. Turkish Journal of Earth Sciences 28 (6): 787-804. doi: 10.3906/yer-1906-13

Özkaymak Ç, Sözbilir H, Uzel B (2013). Neogene–Quaternary evolution of the Manisa Basin: Evidence for variation in the stress pattern of the İzmir-Balıkesir Transfer Zone, western Anatolia. Journal of Geodynamics 65:117-135. doi: 10.1016/j.jog.2012.06.004

Özkaymak Ç, Sözbilir H, Uzel B, Akyüz HS (2011). Geological and palaeoseismological evidence for late Pleistocene-Holocene activity on the Manisa fault zone, western Anatolia. Turkish Journal of Earth Sciences 20 (4): 449-474. doi:10.3906/yer-0906-18

Papanikolaou ID, Roberts GP, Michetti AM (2005). Fault scarps and deformation rates in Lazio–Abruzzo, Central Italy: Comparison between geological fault slip-rate and GPS data. Tectonophysics 408 (1-4): 147-176. doi: 10.1016/j.tecto.2005.05.043

Papazachos, BC. Papazachou CB (1997). The Earthquakes of Greece Editions ZITI, Thessaloniki, pp. 304.

Papazachos BC, Papazachou CB (2003). The earthquakes of Greece. Ziti Publications, Thessaloniki, pp. 273.

Paton S (1992). Active normal faulting, drainage patterns and sedimentation in southwestern Turkey. Journal of the Geological Society of London 149:1031-1044.

Pavlides S (1996). Active faults in Greece J. Earthq. Predict. Res. 5: 422-430.

Pavlides S, Caputo R (2004). Magnitude versus faults' surface parameters: quantitative relationships from the Aegean Region. Tectonophysics 380 (3-4): 159-188. doi: 10.1016/j.tecto.2003.09.019

Pınar N, Lahn E (1952). Türkiye depremleri izahli katalogu. Bayındırlık Bakanlığı, Yapı ve İmar İşleri Reisliği Yayınları, Türkiye: 36 (6) (In Turkish).

Preusser F, Degering D, Fuchs M, Hilgers A, Kadereit A et al. (2008). Luminescence dating: basics, methods and applications. E&G Quaternary Science Journal 57 (1/2): 95-149. doi: 10.3285/eg.57.1-2.5

Ramsey CB (2008). Deposition models for chronological records. Quaternary Science Review 27 (1–2): 42-60. doi:10.1016/j.quascirev.2007.01.019.

Ramsey CB (2009). Bayesian analysis of radiocarbon dates. Radiocarbon 51 (1): 337-360.

Ramsey CB, Higham TFG, Brock F, Baker D, Ditchfield P et al. (2015). Radiocarbon dates from the oxford AMS system: Archaeometry datelist 35. Archaeometry 57 (1): 177-216.

Ramsey CB, Lee S (2013). Recent and planned developments of the program OxCal. Radiocarbon 55 (2): 720-730. doi: 10.1017/S0033822200057878

Reimer PJ, Baillie MG, Bard E, Bayliss A, Beck JW et al. (2009). IntCal09 and Marine09 radiocarbon age calibration curves, 0–50,000 years cal BP. Radiocarbon 51 (4): 1111-1150. IntCal09 and Marine09 radiocarbon age calibration curves, 0–50,000 years cal BP. Radiocarbon 51 (4): 1111–1150. doi: 10.1017/S0033822200034202

Reimer PJ, Bard E, Bayliss A, Beck JW, Blackwell PG et al. (2013). IntCal13 and Marine13 radiocarbon age calibration curves 0–50,000 years cal BP. Radiocarbon 55 (4): 1869-1887. doi: 10.2458/azu_js_rc.55.16947

Richter D, Richter A, Dornich K. (2015). Lexsyg smart-A luminescence detection system for dosimetry, material research and dating application. Geochronometria 42 (1): 202-209. Doi: 10.1515/geochr-2015-0022

Royden LH (1993). Evolution of retreating subduction boundaries formed during continental collision. Tectonics 12 (3): 629-638. doi: 10.1029/92TC02641

Seyitoğlu G, Scott B (1991). Late Cenozoic crustal extension and basin formation in west Turkey. Geological Magazine 128 (2): 155-166. doi: 10.1016/0264-3707(96)00004-X

Seyitoğlu G, Scott B (1996). The age of Alaşehir Graben (west Turkey) and its tectonic implications. Geological Journal 31: 1-11. doi: 10.1002/(SICI)1099-1034(199603)31:1<1::AID-GJ688>3.0.CO;2-S

Sieberg A (1932). Erdbebengeographie. Handbuch der Geophysik, Bd IV, Berlin. (in German)

Slemmons DB, de Polo CM (1986). Active tectonics. Washington (DC): National Academy Press.

Soysal H, Sipahioğlu S, Kolçak D, Altınok Y (1981). Türkiye ve Çevresinin Tarihsel Deprem Kataloğu (2100 B.C.–1900 A.D.). TÜBİTAK raporu, No. TBAG-341.

Sözbilir H, Sümer Ö, Özkaymak Ç, Uzel B, Güler T et al. (2016). Kinematic analysis and palaeoseismology of the Edremit Fault Zone: evidence for past earthquakes in the southern branch of the North Anatolian Fault Zone, Biga Peninsula, NW Turkey. Geodinamica Acta 28 (4): 273-294. doi: 10.1080/09853111.2016.1175294

Sözbilir H, Sümer Ö, Uzel B, Ersoy EY, Erkül F et al. (2009). 17-20 Ekim 2005-Sığacık Körfezi (İzmir) depremlerinin sismik jeomorfolojisi ve bölgedeki gerilme alanları ile ilişkisi, Batı Anadolu. Türkiye Jeoloji Bülteni 51 (2): 217–238 (In Turkish)

Sözbilir H, Uzel B, Sümer Ö, İnci U, Ersoy EY et al. (2008). D-B uzanımlı İzmir fayı ile KD-uzanımlı Seferihisar fayı'nın birlikte çalıştığına dair veriler: İzmir Körfezi'ni oluşturan aktif faylarda kinematik ve Paleosismolojik çalışmalar, Batı Anadolu, Türkiye. Türkiye Jeoloji Bülteni 51 (2): 91–114 (In Turkish).

Spencer JQ, Robinson RA (2008). Dating intramontane alluvial deposits from NW Argentina using luminescence techniques: Problems and potential. Geomorphology 93 (1-2): 144-155. doi: 10.1016/j.geomorph.2006.12.021

Stahl T, Quigley MC, McGill A, Bebbington MS (2016). Modeling earthquake moment magnitudes on imbricate reverse faults from palaeoseismic data: Fox peak and forest creek faults, South Island, New Zealand. Bulletin of the Seismological Society of America 106 (5): 2345-2363

Şengör AMC, Yılmaz Y, Sungurlu O (1984). Tectonics of the Mediterranean Cimmerides: nature and evolution of the western termination of Palaeo-Tethys. Geological Society, London, Special Publications 17 (1): 77-112.

Şengör AMC, Görür N, Şaroğlu F (1985). Strike-slip faulting ve related basin formation in zones of tectonic escape: Turkey as a case study, In: K. Biddle, N. Christie-Blick (eds), Strike-slip Deformation, Basin Formation and Sedimentation. Society of Economic Paleontologists ve Mineralogists Special Publications 37: 227-264.

Tan O, Tapırdamaz MC, Yörük A (2008). The Earthquakes Catalogues for Turkey. Turkish Journal of Earth Science 17: 405-418.

Taymaz T, Jackson J, McKenzie D (1991). Active tectonics of the north and central Aegean Sea. Geophysical Journal International 106 (2): 433-490. doi: 10.1111/j.1365-246X.1991.tb03906.x

Tepe Ç, Sözbilir H, Eski S, Özkaymak Ç, Sümer Ö (2021). Updated historical earthquake catalog of İzmir region (Western Anatolia) and its importance for the determination of seismogenic source. Turkish Journal of Earth Sciences 30: 779-805. doi: 10.3906/yer-2101-14

Tepe Ç, Sözbilir H, Softa M, Özkaymak Ç, Sümer Ö et al (2021b). Paleoseismological Evidence for Late Pleistocene Landslide Triggered by an Earthquake on İzmir Fault, Western Anatolia. In: geological Congress of Turkey; Online, Turkey. pp. 830-831.

Tsodoulos IM, Stamoulis K, Caputo R, Koukouvelas I, Chatzipetros A et al. (2016). Middle–Late Holocene earthquake history of the Gyrtoni Fault, Central Greece: Insight from optically stimulated luminescence (OSL) dating and paleoseismology. Tectonophysics 687: 14-27. doi: 10.1016/j.tecto.2016.08.015

Uzel B, Sözbilir H, Özkaymak Ç (2012). Neotectonic evolution of an actively growing superimposed Basin in Western Anatolia: the inner Bay of İzmir, Turkey. Turkish Journal of Earth Sciences 21: 439-471. doi: 10.3906/yer-0910-11

Uzel B, Sözbilir H, Özkaymak Ç, Kaymakcı N, Langereis CG (2013). Structural evidence for strike-slip deformation in the İzmir–Balıkesir transfer zone and consequences for late Cenozoic evolution of western Anatolia (Turkey). Journal of Geodynamics 65: 94-116. doi: 10.1016/j.jog.2012.06.009

Üner S, Özsayın E, Selçuk AS (2019). Seismites as an indicator for determination of earthquake recurrence interval: A case study from Erciş Fault (Eastern Anatolia-Turkey). Tectonophysics 766: 167-178. doi: 10.1016/j.tecto.2019.06.010

Weismantel O (1891). P Die Erdbeben des vorderen Kleinasiens in geschichtlicher Zeit. PhD, Hoher Philosophischer Fakultat der Universitat Marburg, Frankfurt, Germany (In German).

Wells DL, Coppersmith KJ (1994). New empirical relationships among magnitude, rupture length, rupture width, rupture area, and surface displacement. Bulletin of the Seismological Society of America 84 (4): 974-1002.

Wintle AG, Murray AS (2006). A review of quartz optically stimulated luminescence characteristics and their relevance in single-aliquot regeneration dating protocols. Radiation measurements 41 (4): 369-391.

Zhu L, Akyol N, Mitchell BJ, Sozbilir H (2006). Seismotectonics of western Turkey from high resolution earthquake relocations and moment tensor determinations. Geophysical Research Letters 33 (7). doi: 10.1029/2006GL025842